Max Schmallegger, BSc

Probing the Antioxidant Activity of Resveratrol using CIDNP, CIDEP and EPR

MASTER'S THESIS

to achieve the university degree of

Master of Science

Master's degree program: Chemistry

submitted to

Graz University of Technology

Supervisor

Univ.-Prof. Mag.rer.nat. Dr.phil, Georg Gescheidt-Demner

Institute of Physical and Theoretical Chemistry (PTC)

Graz, March 2016

AFFIDAVIT

I declare that I have authored this thesis independently, that I have not used other than the declared sources/resources, and that I have explicitly indicated all material which has been quoted either literally or by content from the sources used. The text document uploaded to TUGRAZonline is identical to the present master‘s thesis.

Date

Signature

I'd take the awe of understanding

over the awe of ignorance any day.

– Douglas Adams

Acknowledgment

I would like to thank everyone who helped me with my studies and contributed to this work. Special thanks go to

Prof. Georg Gescheidt

for his guidance, countless important discussions and moral support, for the pleasant working environment he provided and most importantly for the fun I had working on my project.

Dmytro Neshchadin

for his support and all the hours he spend explaining the equipment to me, for inspirational discussions, great input to my work and especially for answering all my questions – no matter how clever or unwise they were.

Anna Eibel

for being an awesome office neighbor, study companion, discussion partner for research problems and friend.

Eduard Stadler
Yasmin Bürkl
David Fast
Roman Geier
Anne-Marie Kelterer

for valuable discussions, great fun and a nice working atmosphere.

my friends and family

especially my parents and Leni for their unequivocal support and patience with me.

Abstract

I have investigated the reaction mechanism of the antioxidant resveratrol employing the experimental techniques chemical induced dynamic nuclear polarization spectroscopy (CIDNP), chemical induced dynamic electron polarization spectroscopy (CIDEP) and electron paramagnetic resonance spectroscopy (EPR) as well as density functional theory calculations (DFT). Experimental data from CIDNP and their comparison with DFT calculations suggest that resveratrol reacts with excited triplet states of different photosensitizers either via a hydrogen atom transfer (HAT) or via a concerted electron-proton transfer (EPT). The pH value has a decisive influence on the reaction pathways. EPR spectra of the resveratrol/anthraquinone-2,6-disulfonic acid (AQDS-2,6) system recorded under continuous irradiation confirm these results. The use of anthraquinone-1,5-disulfonic acid (AQDS) in the presence of resveratrol produces spectra corresponding to yet unknown radical species. To obtain a direct fingerprint of the primarily formed radicals, I have utilized time-resolved EPR (CIDEP). Either the photosensitizers benzophenone (BP) and anthraquinone (AQ) or hydroxyl radical generators (photo-Fenton systems) were tested as hydrogen-abstracting agents. Unfortunately, no resveratrol-based radicals could be detected this way. It is assumed that a combination of three factors deteriorates the CIDEP detection of resveratrol radicals: *i*) a low steady-state concentration of the radicals *ii*) the lifetime of resveratrol radicals could be below the detection limit of the spectrometer (< 50 ns) and *iii*) rapid follow-up reactions to non-paramagnetic products.

Kurzfassung

Der Reaktionsmechanismus des Antioxidans Reveratrol wurde mittels der experimentellen Methoden Chemical Induced Dynamic Nuclear Polarization Spektroskopie (CIDNP), Chemical Induced Dynamic Electron Polarization Spektroskopie (CIDEP), Electron Paramagnetic Resonance Spektroskopie (EPR) und Density Functional Theory (DFT) Rechnungen untersucht. Experimentelle Daten aus CIDNP Spektren deuten darauf hin, dass Resveratrol mit dem Triplet-Zustand aromatischer Ketone mittels eines H-Atom Transfers (HAT) oder über einen Elektronen-Protonen Transfer (EPT) reagiert. Welcher der beiden Reaktionsmechanismen dominiert ist abhängig vom pH-Wert bei dem die Messung durchgeführt wird. EPR Spektren des Resveratrol/Anthrachinon-2,6-disulfonsäure (AQDS-2,6) Systems bestätigen diese Resultate. EPR Spektren von Resveratrol in Gegenwart von Anthrachinon-1,5-disulfonsäure (AQDS) liefern Spektren, die von derzeit nicht zuordnenbaren radikalischen Spezies stammen. Die Verwendung der aromatische Ketone Benzophenon (BP) und Anthrachinon (AQ) sowie die Verwendung von Hyroxlradikal-Erzeugern führen zu Spektren ohne detektierbare Signal. Dieses Verhalten lässt sich durch eine geringe steady-state Konzentration der Radikale, bedingt durch schnelle Folgereaktionen, erklären. CIDEP Spektroskopie von Resveratrol in Gegenwart von BP, AQ und AQDS liefert keine Signale, die von radikalischen Spezies stammen – dies lässt sich durch die geringe Lebensdauer (< 50 ns) erklären.

Table of Contents

1 General Introduction

Oxidation and autoxidation is a process occurring in industry and biology. In industrial processes it is responsible for the undesired oxidative degradation of many petroleum-derived materials such as oils, fuels, rubbers and polymers.[1] In biological systems autoxidation is, *e.g.*, responsible for degradation of hydrocarbon moieties and biological materials such as polyunsaturated lipids and steroids[1].

One way of preventing autoxidation processes is the use of antioxidants: Antioxidants are any compounds which slow down or even completely prevent oxidation of another molecule. In biological systems, there is a vast range of different compounds that serve as antioxidants, including enzymes, vitamins such as vitamin A, C or E or polyphenolic compounds.[2,3]

One antioxidant which has gained attention in recent years is resveratrol. The molecule made up from a phenol moiety and a resorcinol moiety is abundant in grapes, peanuts and certain types of berries like mulberries. Resveratrol is suspected to possess beneficial biological functions such as antioxidant activity[4–6] and also cancer chemo-preventive activity.[7,8] In grapes, it is mainly present as its glucoside derivative piceid.[9]

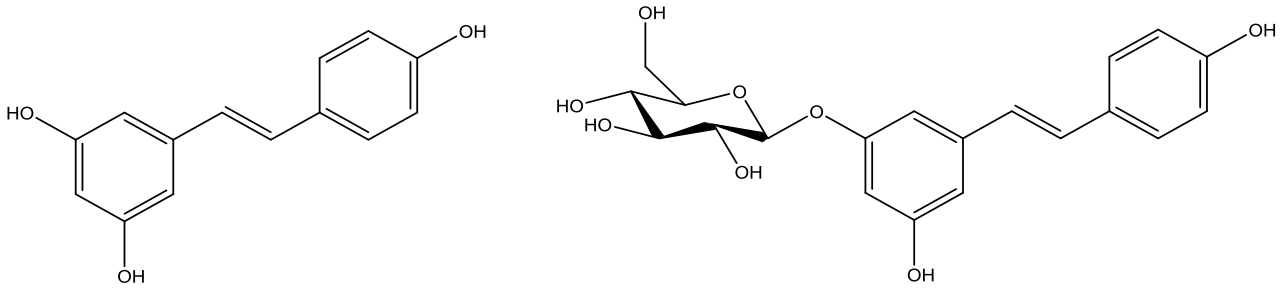

Figure 1 - Structure of resveratrol (3,4',5-trihydroxy-trans-stilbene) (left) and its derivative piceid (right)

Many studies were carried out investigating the antioxidant activity of resveratrol.[2,10–13] These studies use antioxidant assays, laser flash photolysis, spin-trapping in EPR or quantum chemical calculation. However, to my knowledge, there has been no observation of the primary radicals formed from resveratrol being decisive for the antioxidant activity.

In previous works carried out in this working group, mechanistic insight into the antioxidant activity of the polyphenols catechin, gallocatechin, epigallocatechin and epigallocatechingallate was provided.[14,15] Based on this knowledge, I attempted to establish a reaction mechanism for the antioxidant activity of resveratrol using the magnetic resonance-based methods chemically induced dynamic nuclear polarization (CIDNP), chemically induced dynamic electron polarization (CIDEP) and electron paramagnetic resonance (EPR) spectroscopy. These methods provide insight into chemical reactions involving radicals at the molecular level and at an appropriate time regime between *ca.* ns and µs. Density functional theory (DFT) calculations were performed to obtain spectroscopically accessible parameters.

2 Theoretical Background

2.1 Antioxidants

In biological systems, autoxidation is responsible for various undesired reactions like lipid peroxidation and the breakdown of hydrocarbons. The general reaction mechanism of autoxidation is shown in Scheme 1:[16] This chain reaction is initiated by a radical capable of abstracting a H-atom from almost any chemical moiety (equation 1). This results in the formation of a C-centered radical which then undergoes a reaction with molecular oxygen at near-diffusion controlled rates to yield a peroxyl radical (equation 2).[17] The peroxyl radical can further propagate the chain reaction by abstracting a further H-atom (equation 3). Chain termination occurs by radical-radical reactions to yield non-radical (*i.e.* diamagnetic) products (equation 4). The rate determining steps in this process are the peroxide formation (equation 2) and the chain-propagation (equation 3).[18]

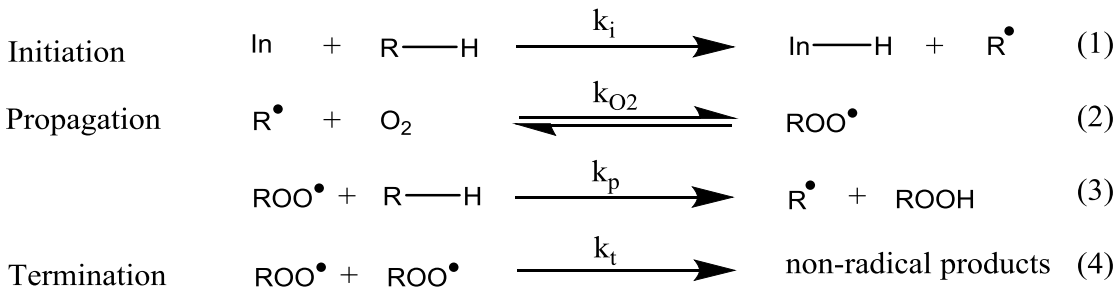

Scheme 1 – Reaction steps in autoxidation-processes

Antioxidants are a class of compounds which slow down oxidative stress. In order to be classified as an antioxidant any compounds must fulfill two conditions: they must be able to delay or prevent the autoxidation or the free radical-mediated oxidation when present in only small quantities compared to the substrate which otherwise would be oxidized.[19] Furthermore the radical generated from the antioxidant must lead to a non-reactive product.[20]

Based on their reaction mechanism, antioxidants are divided into two categories: preventive antioxidants and radical trapping antioxidants.[21,22] Preventive antioxidants

quench the initial radicals and thereby decrease the rate at which radical chains are started. Usually preventive antioxidants decompose peroxides in order to prevent their ability to form chain-initiating hydroxyl radicals.[1] In biology, this is achieved by enzymes such as glutathione oxidase and catalase. In industry organophosphorus and organosulfur compounds are used as preventive antioxidants.

Radical-trapping antioxidants (also called chain-breaking antioxidants) react with chain-carrying peroxyl radicals to yield unreactive radicals according to (equation 5) and (equation 6) in Scheme 2.

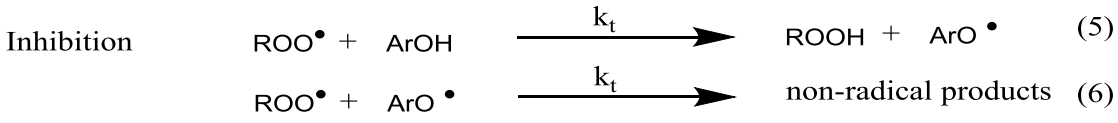

Scheme 2 - Inhibition of autoxidation by phenolic radical-trapping antioxidants

The best known type of radical-trapping antioxidants are phenols (ArOH) which react with peroxyl radicals via the transfer of the phenolic hydrogen atom yielding phenoxyl radicals. These phenoxyl radicals are in general persistent as they are stabilized by intramolecular hydrogen bonding and resonance stabilization. This means they slowly react with O_2 and are eventually 'consumed' by another peroxyl radical.[23]

In order to determine antioxidant activity, a number of different assays have been introduced. These assays are designed to measure the total antioxidant activity of body fluids,[24,25] food extracts[26,27] and pure compounds.[12] These methods are based on the generation of various radicals and spectrophotometric measurements either at a fixed time or over a time range.[2] Two different approaches are applied: the inhibition assay in which the antioxidant activity is determined by the extent to which a pre-formed radical is scavenged and assays in which the antioxidant system is present whilst the formation of the free radical.[2]

One polyphenol which is of particular interest is resveratrol. Resveratrol (3,4',5-trihydroxy-trans-stilbene) is a plant phytoalexine. It is frequently found in plants such as

grapes, berries and peanuts where it is produced as a reaction to injury or bacterial and fungal infection.[28,29] Resveratrol has been associated with many beneficial biological activities such as inhibition of cancer promotion and propagation and is furthermore suspected to yield protection against cardiovascular disease.[30–32]

2.2 Resveratrol

The antioxidant activity of resveratrol is strongly related to its capability of scavenging reactive oxygen species (ROS) like peroxyl radicals ($ROO^{\bullet}$), hydroxyl radicals ($HO^{\bullet}$) and superoxide radicals ($O_2^{\bullet -}$).[33] By scavenging these radicals, resveratrol prevents the peroxidation of lipids and proteins.

When looking at the structure of resveratrol, it is obvious that there are two possible sites for hydrogen abstraction which determine the antioxidant activity (Scheme 3): the hydroxyl group on the phenol moiety (A-Ring) and the two hydroxyl groups in the resorcinol moiety (B-Ring) giving rise to two different uncharged radical species $\mathbf{A}^{\bullet}$ and $\mathbf{B}^{\bullet}$. Furthermore resveratrol could react by donating an electron to a ROS yielding a radical cation $\mathbf{AB}^{\bullet +}$. Another possible reaction pathway for resveratrol serving as an antioxidant is the donation of an electron to a suitable acceptor followed by a proton transfer, resulting in one of three possible radical anion species, $\mathbf{A}^{\bullet}\mathbf{B}^{-}$, $\mathbf{A}^{-}\mathbf{B}^{\bullet}$ and $\mathbf{BB}^{\bullet -}$.

Several studies have been carried out concerning the radicals formed from resveratrol: experiments investigating the reaction of resveratrol with hydroxyl radicals suggest the formation of phenoxyl radical $\mathbf{A}^{\bullet}$ as the most stable radical product.[34] Pulse radiolysis experiments come to the same conclusion.[35] Density functional theory studies underpin that radical $\mathbf{A}^{\bullet}$ is more stable than radical $\mathbf{B}^{\bullet}$.[13]

However, to my knowledge, there are no studies concerning the direct formation of radicals in processes involving resveratrol as an antioxidant. Therefore there is little knowledge on whether this more stable species A• is also preferentially formed, or if hydrogen abstraction also occurs on the B-Ring followed by charge redistribution yielding $\mathbf{A}^{\bullet}$ or even if there is another process involved.

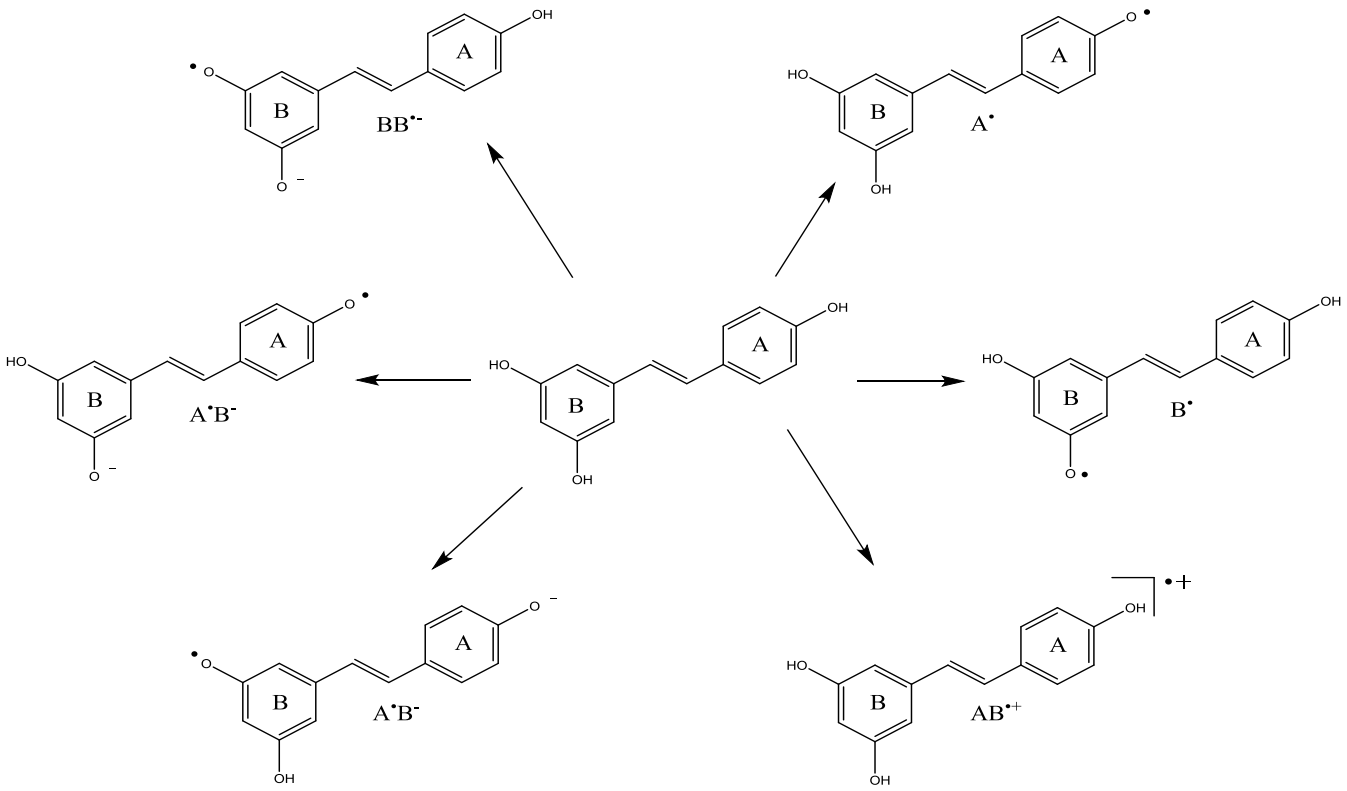

Scheme 3 – Possible radical species formed from resveratrol

2.3 **Reactivity of Carbonyl Triplets**

As mentioned above, the antioxidant activity of resveratrol is strongly related to its capability of scavenging ROS. As the production of ROS can be difficult and these species display only short lifetimes[36] different approaches have been taken to mimic the reactivity of ROS.

One of these approaches is the use of excited carbonyl triplets: these triplet states react either via an hydrogen atom transfer (HAT)[37] or via concerted electron-proton transfer (EPT)[38] and exhibit reactivity comparable to those of reactive oxygen species (ROS).[39–41] The behavior of n,π* carbonyl triplets and its similarity to alkoxyl radicals has been highlighted in various studies.[18,42,43]

Excited triplet states of (aromatic) ketones are well known to be efficiently quenched by phenols, both in aprotic and protic solvents.[44] This quenching results in the reduction of the triplet ketones to ketyl radicals. Accordingly, the phenols are oxidized to phenoxyl radicals. This reaction can occur either via a hydrogen transfer or via an electron transfer followed by a proton transfer. The quenching of aromatic ketone triplets by phenol was found to be a very fast process with rate constants ranging from 10^7 M^{-1} s^{-1} in benzene to 10^9 M^{-1} s^{-1} in wet acetonitrile.[37]

In the case of phenols, the reaction of carbonyl triplets is suspected to proceed via a reversible hydrogen abstraction from the phenol to the triplet carbonyl, rather than by undergoing electron transfer (Scheme 4).[45]

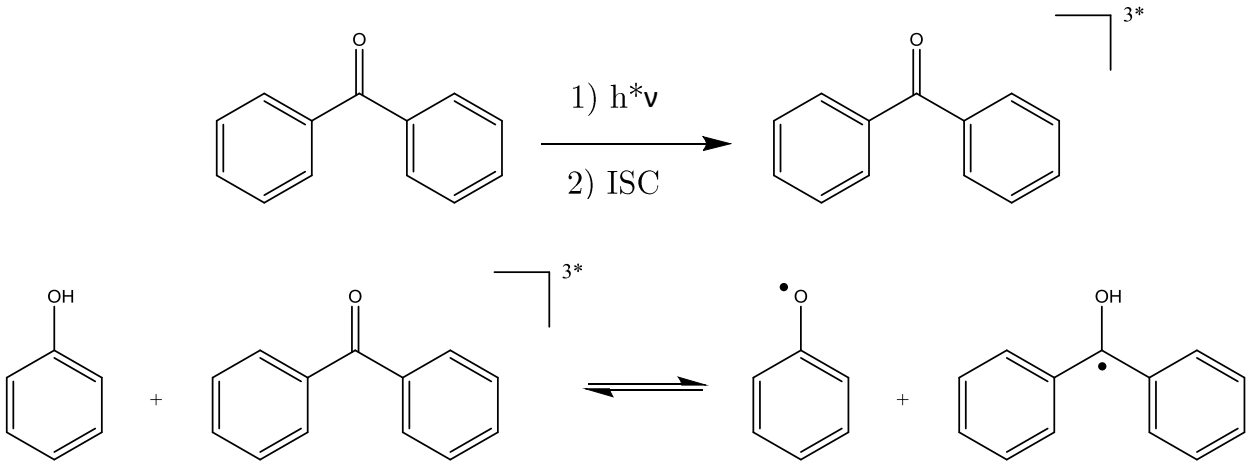

Scheme 4 - Generation of the triplet state of benzophenone and hydrogen abstraction from phenol by this triplet state

Two aromatic triplets which are frequently used for testing antioxidative properties are benzophenone (BP) and anthraquinone-1,5-disulfonic acid (AQDS). They are ideal reactants for this purpose since their triplet state displays HAT reactivity very similar to that of ROS.[39,40,46] Upon irradiation with near-UV light BP and AQDS undergo excitation to the excited singlet state, followed by intersystem-crossing to the triplet state.

2.4 Fenton- and photo-Fenton Reactions

Hydrogen peroxide is a strong oxidant which is frequently used for a number of applications such as the use as bleaching agent or the treatment of various organic and

inorganic pollutants. However, H_2O_2 alone often is not sufficient due to its low reaction rates at reasonable concentrations.[47] A number of different methods like the addition of transition metal salts, UV-irradiation or the addition of ozone (O_3) have been established to activate H_2O_2 and form the hydroxyl radical ($\bullet OH$) which is a strong oxidant.[47]

- Hydrogen peroxide and ozone

$$O_3 + H_2O_2 \rightarrow OH\bullet + O_2 + HO_2^{\bullet} \quad (7)$$

- Hydrogen peroxide and iron salts

$$Fe^{2+} + H_2O_2 \rightarrow Fe^{3+} + OH\bullet + OH^- \quad (8)$$

- Hydrogen peroxide and UV-light

$$H_2O_2 \xrightarrow{h*\nu} 2\,OH\bullet \quad (9)$$

Fenton's reagent was discovered more than 100 years ago.[48] It is a mixture of hydrogen peroxide and ferrous iron which creates OH radicals according to (equation 8).

According to literature, the term photo-Fenton reaction can refer to two different phenomena: either to the reaction of Fe(III) complexes like Fe(III)oxalate which, upon irradiation, release Fe(II) and therefore start the Fenton reaction according to (equation 8).[49] Or it refers to reactions in which a chemical compound is irradiated and then selectively releases the $\bullet OH$ radical. Compounds of this type are generally regarded as non-specific hydroxyl radical generators. One example of such a non-specific hydroxyl radical generator is *N*-hydroxypyridine-2(1H)-thione (N-HPT). Upon irradiation with UV-light, N-HPT undergoes homolytic bond cleavage yielding a 2-pyridylthiyl radical alongside a hydroxyl radical (Scheme 5).[50]

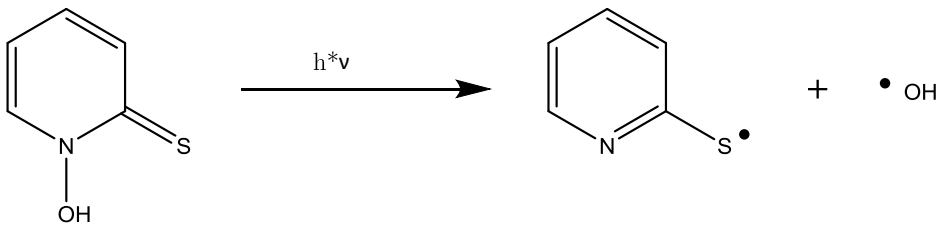

Scheme 5 – reaction scheme for the release of $\bullet OH$ radical by N-HPT upon irradiation

3 Experimental Techniques

3.1 Electron Paramagnetic Resonance

Electron paramagnetic resonance (EPR) spectroscopy, sometimes also referred to as electron spin resonance (ESR) spectroscopy, was first described almost 70 years ago. The technique is based on the absorption of electromagnetic radiation by a sample placed inside a magnetic field. As the name already implies, paramagnetic species are investigated using EPR. The signals in EPR give rise to information about all nuclei-electron interactions via the so-called hyperfine splitting pattern.

When placed inside an external magnetic field B_0, electrons align due to their magnetic moment μ_e in one of two possible ways: either parallel – which is described as $M_s = -\frac{1}{2}$ - or anti-parallel, described as $M_s = +\frac{1}{2}$, to the external magnetic field. These two configurations are different in energy, with the parallel state being lower. This effect is called the Zeeman effect and forms the basis of EPR spectroscopy (Figure 2). According to the Boltzmann distribution, the two different energetic levels are not equally populated inside the magnetic field, allowing the transition between the two states.[51]

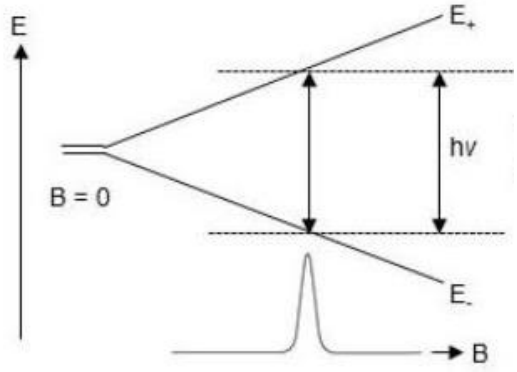

Figure 2 – Splitting of electronic levels in the presence of an external magnetic field due to the Zeeman effect

The energy difference between the two states is given by the following equation which is also known as the EPR resonance condition[52]

$$\Delta E = E_+ - E_- = g * \mu_B * B = h * \nu \qquad (15)$$

with the individual parameters being:

- E_+ energy of the higher lying electronic state
- E_- energy of the lower lying electronic state
- g g-factor of the radical
- μ_B Bohr magneton; $9.274*10^{-24}$ JT^{-1}
- B magnetic field strength
- h Planck's constant; $6.626*10^{-34}$ Js
- ν frequency of the microwave

In organic radicals, the g-factors are usually rather similar to the value for the free-electron ($g_e = 2{,}0023193043617$).[53] The deviations from this value arise from the spin-orbit coupling by the elements surrounding the radical center.

Further information in EPR spectra arises from the hyperfine interaction: unpaired electrons interact with the surrounding nuclei. These nuclei mostly possess magnetic moments which produce a local magnetic field B_I at a nucleus. This causes an additional splitting of the Zeeman energy levels. The local magnetic field B_I and the applied external magnetic field again can either align or oppose each other. If they align, the field of resonance is shifted to lower energy. Correspondingly, if they are opposite, the field of resonance is shifted to higher energy. This is depicted in Figure 3.[52] The overall splitting depends on the number of nuclei as well as their nuclear spin I. For n equivalent nuclei, 2*n*I+1 lines are present in the EPR spectrum.

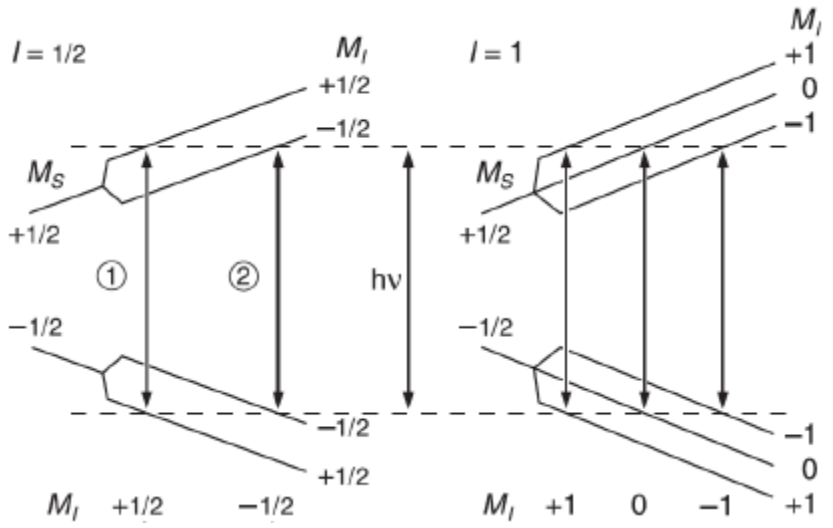

Figure 3 – Further hyperfine splitting of the electronic Zeeman levels for I = ½ (left) and I = 1 (right)

3.2 Chemically Induced Dynamic Electron Polarization

CIDEP spectroscopy (sometimes also called time resolved electron paramagnetic resonance spectroscopy) is an experimental technique based on EPR spectroscopy and allows the detection of radicals on a nanosecond-to-microsecond timescale.[54] At these time scales, the population of the energy levels differs from the Boltzmann distribution giving rise to enhanced absorption or emission. These polarized signals originate from two different mechanisms – the radical pair mechanism (RPM) and the triplet mechanism (TM). From CIDEP spectra it is possible to obtain information on the spin multiplicity of the precursor and the structure of the primarily formed radicals. It is also possible to carry out kinetic studies employing line-width methods.[55]

3.2.1. The Radical Pair Mechanism

Radical pairs can be created either by homolytic cleavage of a bond, by electron transfer or by hydrogen atom transfer. In CIDEP spectroscopy, these processes are induced thermally or photochemically. In both cases, the spin multiplicity of the precursor molecule is conserved. This means thermally generated radical pairs are usually born in the singlet state (except for rare cases in which the precursor molecule is in a triplet

ground state). In the photochemical generation of radical pairs also triplet precursors occur leading to radical pairs formed in the triplet state. For completeness, it should be mentioned that there is also a third possibility to generate a radical pair: by the encounter of two separate free radicals. If two such radicals meet, they can form a radical pair either in the singlet the triplet states. However, since singlet pairs will mostly recombine very rapidly, the triplet character dominates for radical pairs formed this way.[56]

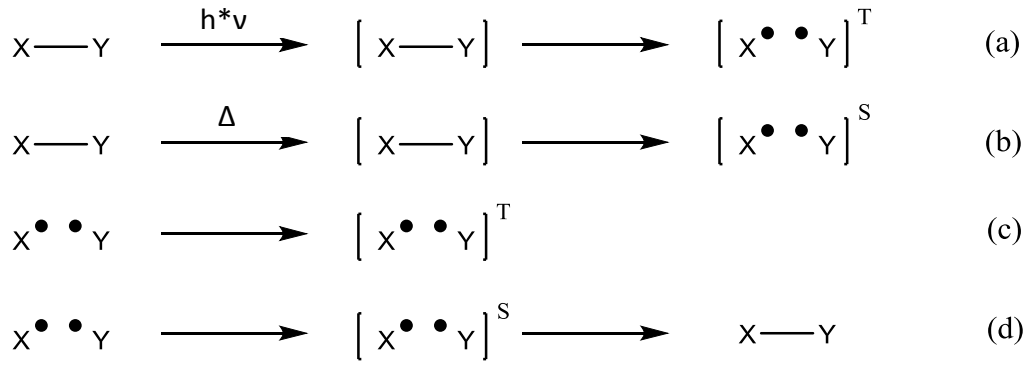

Scheme 6 - Radical pair formation by photochemical reaction (a), thermal reaction (b) or the recombination of free radicals (c), (d)

In radical pairs, the two radicals cannot be regarded to as separate chemical species if the distance between them is small enough (spin coupled radical pairs). At close inter-radical distances the two radicals are 'aware' of each other, and therefore their spin state cannot be chosen independently. This spin correlation is due to the exchange interaction, a purely quantum mechanical effect.[57]

Intersystem crossing between triplet state and singlet state can occur in a process called singlet-triplet mixing (S-T mixing). This S-T mixing depends on the inter-radical distance r. At small distances r the triplet and the singlet state possess a large energy difference due to high exchange interactions. At larger distances the singlet state and the triplet states are degenerate, allowing the interconversion between them (Figure 5).[58] A representation of the S-T mixing process is given by the vector model, as it is shown in Figure 4.

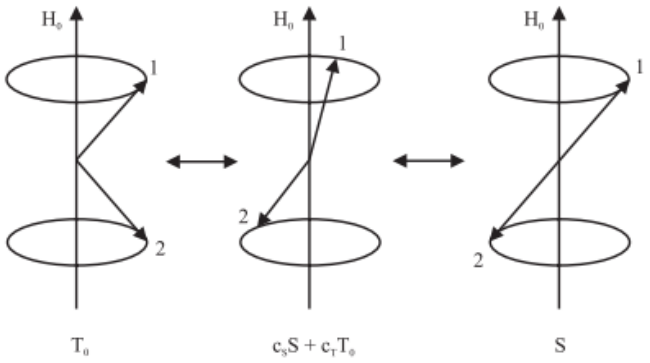

Figure 4 - Vector representation of the Singlet Triplet Mixing

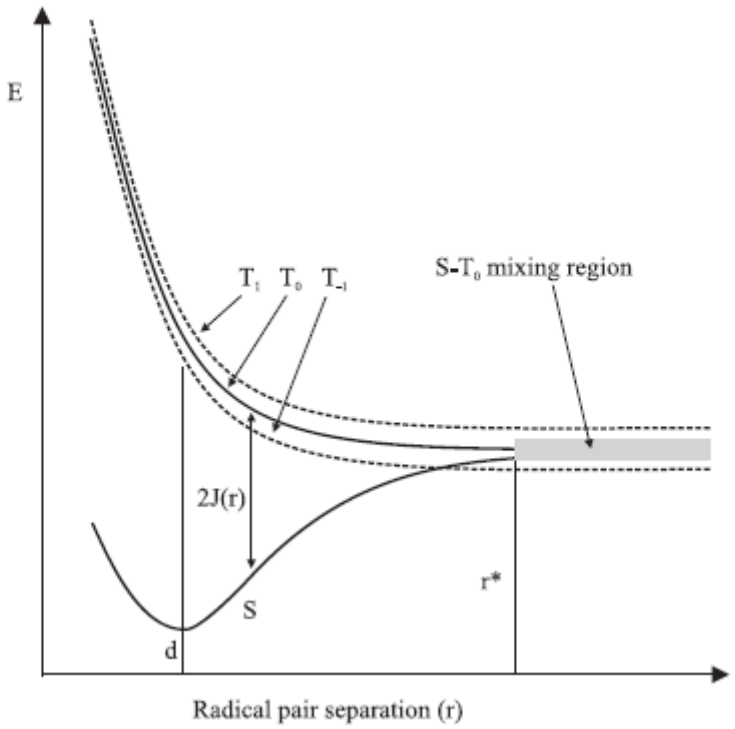

Figure 5 – Energy level diagram of a radical pair in the presence of an external magnetic field as function of the inter-radical distance

Polarized signals originating from the radical pair mechanism can exhibit different polarization patterns: All signals can show either enhanced absorption (A) or emission (E) (net effect). It is also possible that both signals of enhanced absorption and emission are observed within the same multiplet. (multiplet effect).

3.2.2. The Triplet Mechanism

The triplet mechanism can be detected in cases when the radical pair is generated photochemically, as a triplet precursor is required. After excitation of the molecule to its excited singlet state, the polarization is built up during the intersystem crossing to the triplet state. Due to the non-degeneracy of the three magnetic triplet states at high magnetic field, the three levels are populated to different extends resulting in a polarization. The size of this polarization depends on several parameters:[59]

- the rotational correlation time of the precursor molecule
- the zero field splitting constant of the excited triplet states
- the lifetime of the triplet state
- the magnetic field which is applied

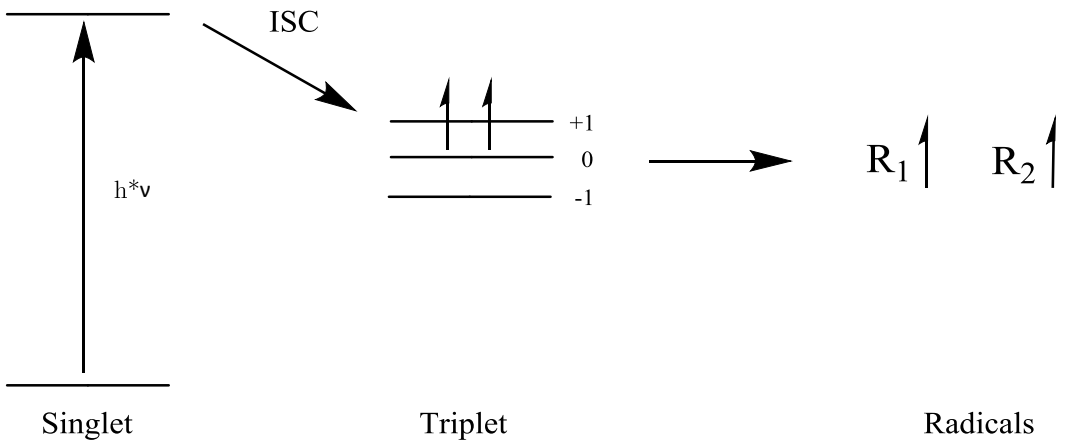

Figure 6 – Mechanistic representation of the selective population due to the triplet mechanism in CIDEP experiments

In Figure 6, the preferred population of the T_{+1} state leads to emission signals. Accordingly, spin polarization originating from triplet mechanism leads to signals of identical phase and enhancement.

3.2.3. Experimental Setup

CIDEP spectra can be recorded two ways: using either continuous wave EPR (cw-EPR) or the more recent Fourier-transformation EPR (FT-EPR). In this work, cw-EPR was employed. The experimental setup for these experiments usually consists of a laser serving as a nano-second light source and direct detection using an X-Band EPR spectrometer. The signal acquisition is synchronized to the laser trigger and recorded using a digital oscilloscope. The whole setup is controlled by a PC.

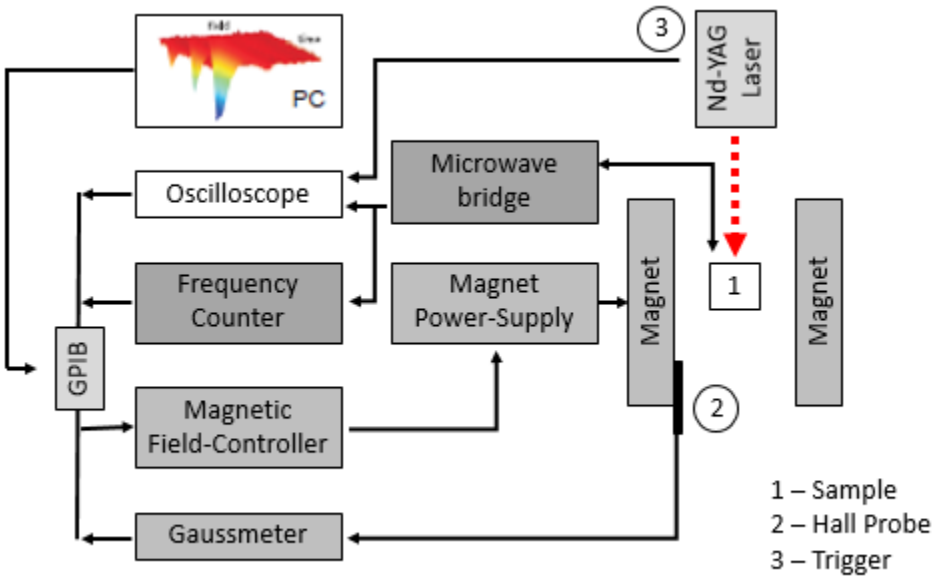

Figure 7 – Experimental Setup of a CIDEP spectrometer

3.3 Chemically Induced Dynamic Nuclear Polarization

Chemically Induced Dynamic Nuclear Polarization (CIDNP) is an effect observable in Nuclear Magnetic Resonance (NMR) experiments when fast radical reactions are taking place. In contrast to CIDEP, not the radical species itself is detected, but signals of the follow-up products bearing information about the radical reaction pathway.

The effect which is responsible for the abnormal intensities in CIDNP spectroscopy is the RPM and is analogous to the effect observed in CIDEP (see chapter 3.2.1). As a result of the interaction between unpaired electrons and nuclear spins, radical pairs are formed in

a polarized state and therefore non-Boltzmann effects on the applied timescale dominate the spectrum. Thus, signals of enhanced absorption or emission are observed in CIDNP experiments.

A representation of the triplet mechanism leading to the formation of polarized signals in CIDNP experiments is presented in Figure 7. The radical pair is formed either from a singlet or triplet precursor. It then can undergo a nuclear-spin selective singlet triplet mixing. This singlet-triplet mixing process is analogous to CIDEP and can be described using the vector model. In the last step, singlet and triplet radical pairs undergo different subsequent reactions, leading to the products observed. Cage products are formed by recombination of the initial radical, whereas escape products are formed outside the solvent cage by a radical pair which has diffused apart. This means that singlet-triplet mixing is required for the formation of cage products from triplet precursors.

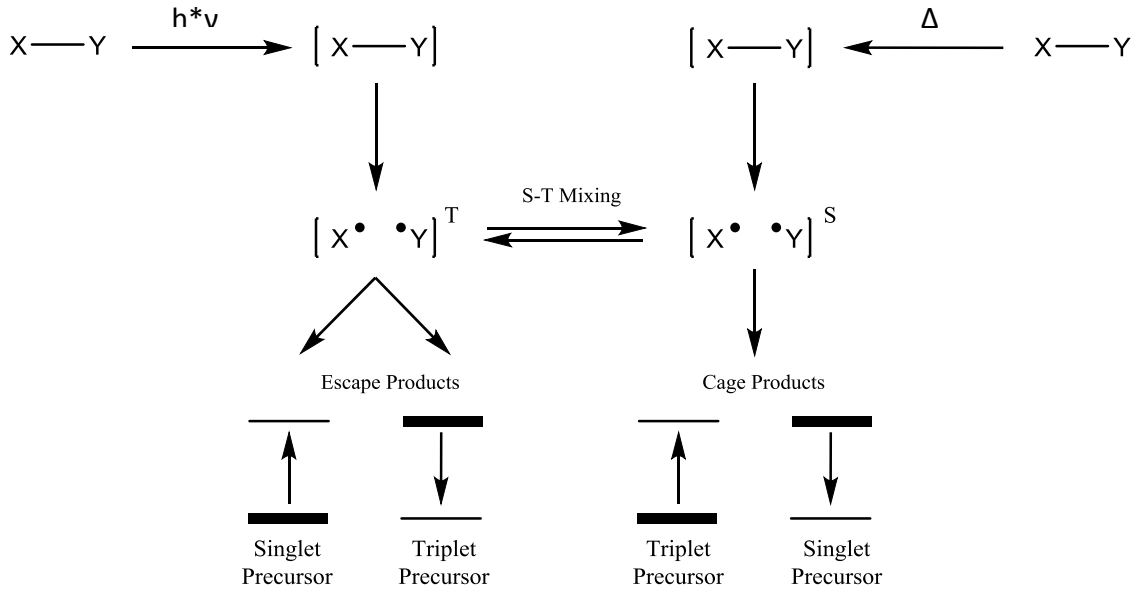

Figure 8 - Reaction scheme of the radical pair mechanism of CIDNP

The rate of S-T mixing is proportional to the difference of the Larmor frequencies $\Delta\omega$ of the two electron spins as it is shown in (equation 10):[60] directly after the formation of the radical pair, the spin state of the system is the same as of its precursor. After a certain time the two radicals will diffuse apart making the exchange interaction negligible. The

two radicals are no longer constrained to preserve their relative orientation and they start to precess independently in the magnetic field. If the two radicals are different, they will precess with different Larmor frequencies resulting in singlet-triplet mixing. The difference between the Larmor frequencies is given by:

$$\Delta\omega = \omega_1 - \omega_1 = \frac{1}{2}\left[H_o \Delta G\, \beta_e h^{-1} + \sum_{i=1}^{n} a_{1i} m_{1i} - \sum_{j=1}^{k} a_{2j} m_{2j}\right] \qquad (10)$$

The first term of the equation arises from spin-orbit interaction, whilst the other two terms are responsible for electron coupling – which is the same as hyperfine splitting in EPR. As an example, a radical pair formed in the T_0 state is given in which only one radical carries magnetically active nuclei with $|m_{1i}| = ½$, $\Delta g > 0$, $a_{1i} > 0$. For such a radical pair, there are two possible values for $\Delta\omega$ depending on the spin orientation:

$$\alpha;\ m_{1i} = +\frac{1}{2}, \qquad \Delta\omega_+ = \frac{1}{2}\left[H_o \Delta G\, \beta_e h^{-1} + \frac{1}{2} a_{1i}\right] \qquad (11)$$

$$\beta;\ m_{1i} = -\frac{1}{2}, \qquad \Delta\omega_- = \frac{1}{2}\left[H_o \Delta G\, \beta_e h^{-1} - \frac{1}{2} a_{1i}\right] \qquad (12)$$

This means that the rate of Singlet-Triplet Mixing depends on the nuclear spin orientation.

3.3.1. Kaptein Rules

In 1971, R. Kaptein proposed a set of simple rules which allow the qualitative interpretation of CIDNP spectra.[61] These rules are based on the nature of the precursor, the formation of either cage or escape products, the difference in g-values of the two radicals and the sign of the hyperfine coupling constant (hfc) for the net effect.

$$\Gamma_{NE} = \mu * \varepsilon * sgn\, \Delta g * sgn\, a_i \qquad (13)$$

For the multiplet effect, additionally the sign of the coupling constant is taken into account.

$$\Gamma_{ME} = \mu * \varepsilon * sgn\, a_i * sgn\, a_j * \delta_{ij} * sgn\, J_{ij} \qquad (14)$$

The signs of all constants and variables in the two equations (13) and (14) are as follows;

- μ + Triplet precusor
  − Singlet precursor
- ε + Cage product
  − Escape product
- $sgn\, \Delta g$ sign of g_1-g_2; g_1 is the g-factor of the radical at which the nucleus of interest is located
- $sgn\, a_i$ sign of hfc of nucleus i
- $sgn\, a_j$ sign of hfc of nucleus j
- δ_{ij} + if nuclei i and j are located on the same radical
  − if nuclei i and j are located on different radicals
- $sgn\, J_{ij}$ sign of nuclear coupling constant between nuclei i and j
- Γ_{NE} + Absorption
  − Emission
- Γ_{ME} + Emission/Absorption
  − Absorption/Emission

3.3.2. Experimental Setup

The radical pair inside the NMR spectrometer is generated either thermally or photochemically. In this work, the photochemical approach was employed. The setup consists of a Bruker 200 MHz NMR spectrometer and a BrilliantB Nd/YAG laser operating at 355 nm. The setup for CIDNP experiments is essentially the same as in NMR,[62] only with the addition of a quartz rod that is used to guide the light of the laser to the NMR tube inside the spectrometer (Figure 8).

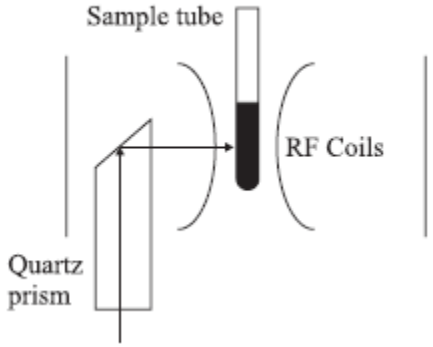

Figure 9 – Arrangement of NMR probehead in CIDNP experiments

3.4 Density Functional Theory

Density functional theory (DFT) is a computational quantum mechanical method. Other than for so called *ab-initio* methods, which solve the Schrödinger equation for a chemical system, in DFT calculations the complex many-body wave-function resulting from the Schrödinger equation is substituted by an effective one-body system known as the electron density. The electron density only depends on three spatial coordinates.[63]

The theory of DFT calculations is based on the work of Thomas and Fermi and was further developed by Kohn, Sham and Hohenberg in the 1960s. Due to its nature of reducing the calculations to an effective one-body system, DFT is computationally less demanding than other methods leading to results with comparable accuracy.

For any given electronic system, the electron probability density ρ can be used to describe the total energy of this system. If the system consist of n electrons, the total electron density within the volume d^3r around a certain point in space r is given by $\rho(r)$. Since electrons cannot be distinguished, the probability of finding any electron at r is given by the probability of finding a certain electron times **n** as shown in equation (16).[64]

$$\mathrm{n} = \int \rho(\mathrm{r}) d^3r \qquad (16)$$

4 Experimental Part

4.1 Materials and Solvents

Resveratrol was received from TCI Chemicals and was used without any further purification. The photosensitizers benzophenone (Fluka, ≥ 99%), anthraquinone (Fluka, ≥ 99%), anthraquinone-1,5-disulfonic acid (TCI Chemicals, ≥ 98%) and anthraquinone-2,6-disulfonic acid (Fluka, ≥ 98%) were used as received. Iron(II)-chloride tetrahydrate ($FeCl_2$*$4H_2O$, ≥ 98%), hydrogen peroxide (H_2O_2; Roth, 30% stabilized in H_2O) and 2-mercaptopyridine N-oxide (Sigma-Aldrich, ≥ 99%) were used without additional treatment. Resorcinol (Sigma-Aldrich, ≥ 99%) and Phenol (Merck, ≥ 95%) were employed as received.
The solvents acetonitrile (Sigma-Aldrich, ≥ 99,9%), acetronitrile-d_3 (Euriso-Top, ≥ 99,8%) and D_2O (Sigma-Aldrich, ≥ 99,9%) were employed without further purification. For aqueous samples, deionized water was employed.

4.2 CIDNP

^{1}H-CIDNP experiments were carried out on a 200 MHz Bruker AVANCE DPX spectrometer featuring a custom-made CIDNP probehead. A Quantel Nd:YAG Brilliant B laser (355 nm, ~ 60 mJ/pulse, pulse length ~ 8−10 ns) operating at 20 Hz was employed as light source. The timing sequence of the experiment consists of a series of 180° radiofrequency (RF) pulses (applied to suppress the normally present NMR intensities), the laser flash, the 90° RF detection pulse and the acquisition of the free induction decay. (FID). Samples were prepared in 1:1-mixtures of deuterated acetonitrile and H_2O or deuterated acetonitrile and D_2O and deoxygenated by bubbling with argon before the experiment.

4.3 EPR

A Bruker EMX X-band spectrometers (100 kHz field modulation) was used to record cw-EPR spectra. Typical experimental conditions were 2 mW microwave power and 0.15 mT field modulation. All solutions for EPR measurements were saturated with argon by

bubbling for 10 minutes. Samples of resveratrol and photosensitizers as well as samples of photo-Fenton + resveratrol reagents were pumped through a quartz cell positioned inside the cavity of the EPR spectrometer and continuously irradiated with light from a Hamamatsu Lightingcure LC4 lamp (λ_{max} 365 nm). Samples of resveratrol with Fenton's reagent were pumped through the flat cell using a syringe pump mounted with three syringes containing the individual solutions. Spectra were analyzed with the WinEPR software (Bruker) as well as with WinSim[65] public domain program.

4.4 CIDEP

Continuous-wave CIDEP experiments were performed on a Bruker ESP 300E X-band spectrometer (unmodulated static magnetic field) equipped with a 125 MHz dual channel digital oscilloscope (Le Croy 9400). The light source a Nd:YAG laser operated at the third harmonic (InnoLas Spitlight 400, 355 nm, operating at 20 Hz, 6-8 mJ/pulse, 8 ns). The whole setup is controlled by the fsc2 software developed by Dr. J. T. Toerring (Berlin). Spectra were recorded by acquiring the accumulated (50 accumulations) time responses to the laser pulses at each magnetic field value of the chosen field range (field steps: 0.5 G). Argon-saturated solutions of the samples were pumped through a quartz flat cell positioned in the cavity of the EPR spectrometer using a flow system.

4.5 Density Functional Calculations

For all Density Functional Theory calculations the restricted Becke's three parameter hybrid functional with the nonlocal Lee, Yang and Parr gradient-corrected correlation functional (B3LYP) was used.[66,67] For geometry optimization the Def2TZVPP basis set was employed.[68] The calculation of EPR coupling constants was realized using the IGLO-II basis set.[69] In order to include the solvent effects into the calculations, the Conductor-like Screening Model (COSMO) was used in all computations.[70] All calculation were performed using the ORCA software package.[71]

5 Results and Discussion

5.1 CIDNP measurements

5.1.1. Resveratrol in the presence of benzophenone

^{1}H NMR spectroscopy of resveratrol and benzophenone in a 1:1 mixture of CD_3CN/D_2O yield the spectrum presented in Figure 11. In the aromatic region of the spectrum (ranging from 6.0 ppm to 8.0 ppm) signals corresponding to benzophenone and resveratrol are clearly visible. The other two large peaks present in the spectrum at around 4.5 ppm and 2.0 ppm correspond to non-deuterated traces of the solvents D_2O and CD_3CN, respectively. The protons of the hydroxyl groups are not visible in the NMR spectrum due to the exchange with solvent molecules.

The assignment of the signals corresponding to resveratrol is straight forward as shown in Figure 12. The CIDNP spectrum exhibits polarizations of comparable size and intensity on the H-atoms 2, 4, 6, 7, 11 and 13 as well as some smaller polarizations on the H-Atoms 8, 10 and 14.

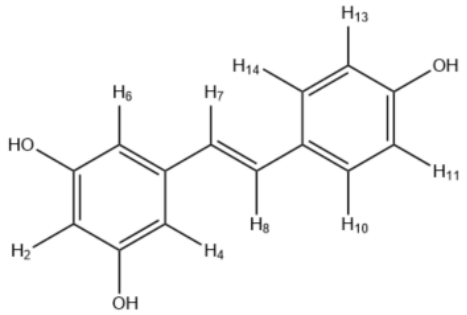

Figure 10 - Numbering of H-Atoms of resveratrol used for the assignment of NMR signals

The ^{1}H NMR spectrum of resveratrol and benzophenone in a 1:1 mixture of CD_3CN/H_2O (Figure 15) yield the identical signals as in CD_3CN/D_2O. The pattern of the peaks in the spectrum exhibiting emissive signals is caused by the high water content. The very high number of H-atoms in the sample leads to the over-modulation of the receiver. Comparison of two CIDNP spectra recorded in different binary solvent mixtures shows similar polarization patterns and signal intensities.

Notably, there are differences between the NMR spectra before and after the CIDNP experiments: In the spectrum recorded after the CIDNP experiment, new peaks are observable which correspond to the cis-isomer of resveratrol since this isomerization is known to be triggered at 355 nm.[72] These newly occurring peaks are represented by a (#) in Figure 14.

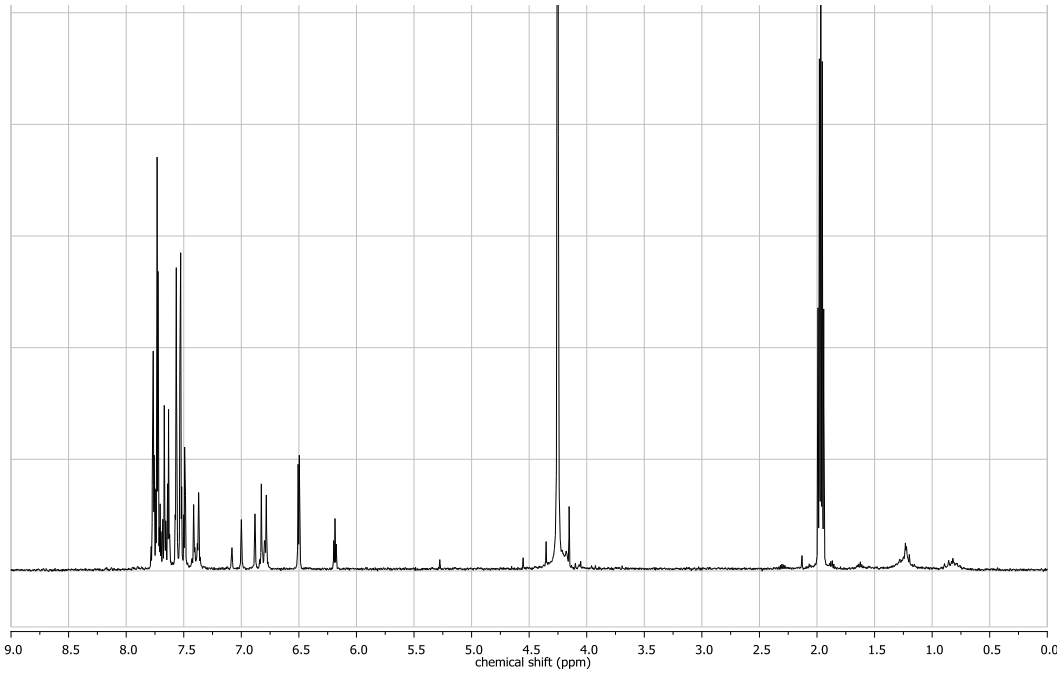

Figure 11 - 1H-NMR spectrum of resveratrol and benzophenone recorded in CD3CN/D2O 1:1

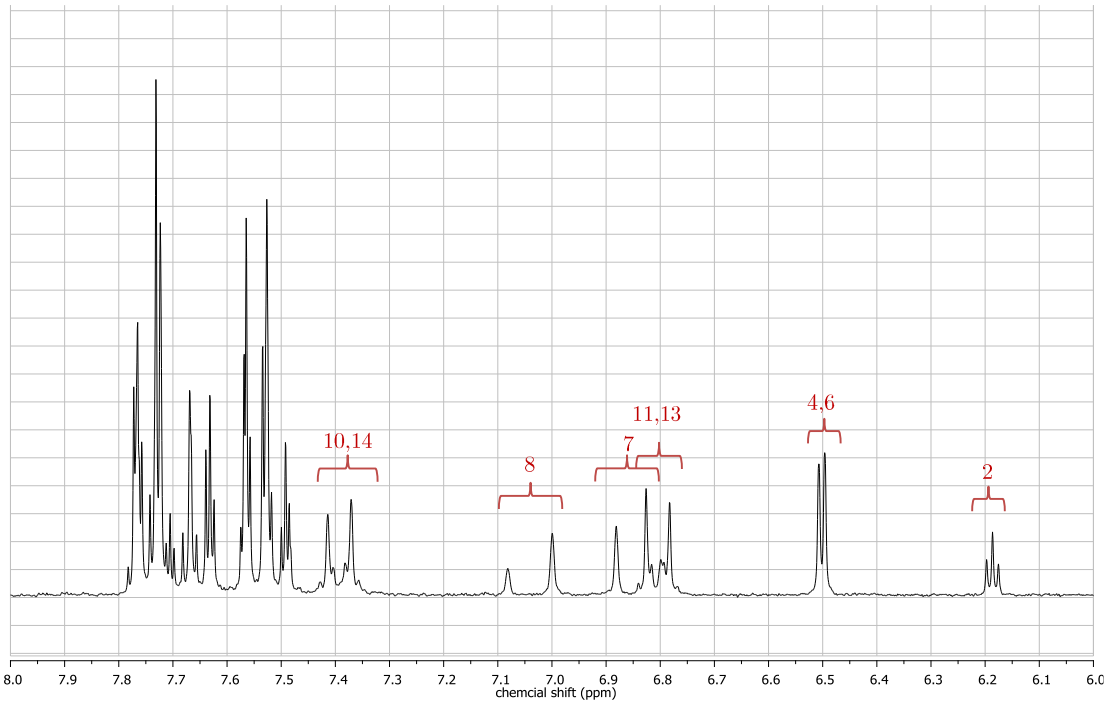

Figure 12 – Aromatic region of the 1H-NMR spectrum of resveratrol and benzophenone in recorded in a 1:1 CD3CN/D2O mixture

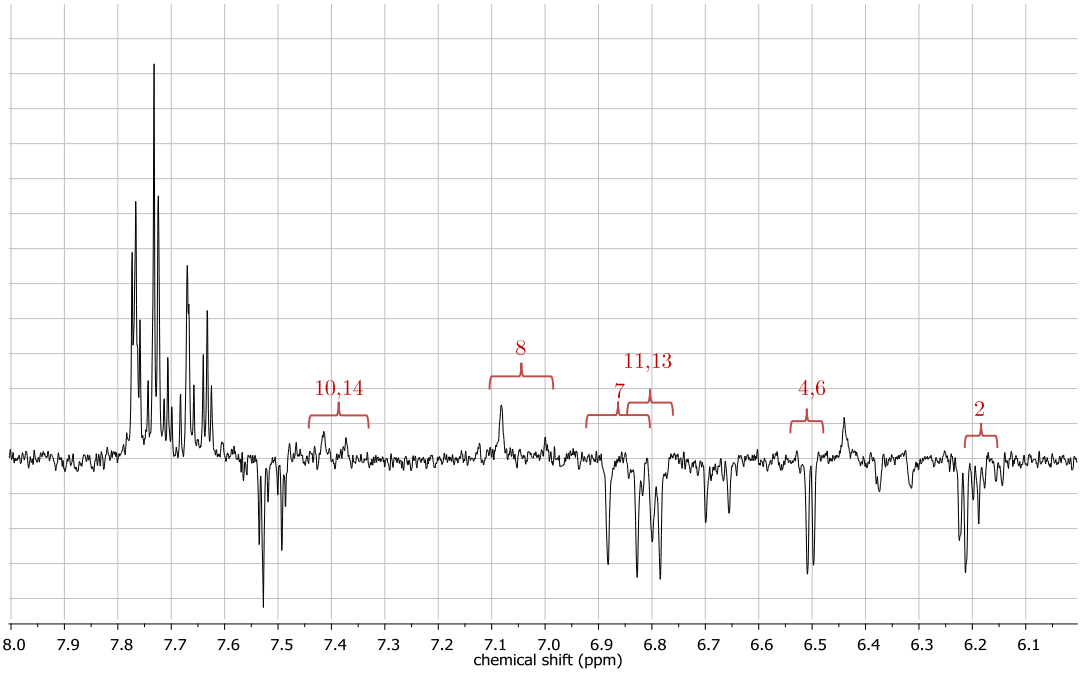

Figure 13 – Aromatic region of the ^{1}H-CIDNP spectrum of resveratrol and benzophenone recorded in a 1:1 CD3CN/D2O mixture

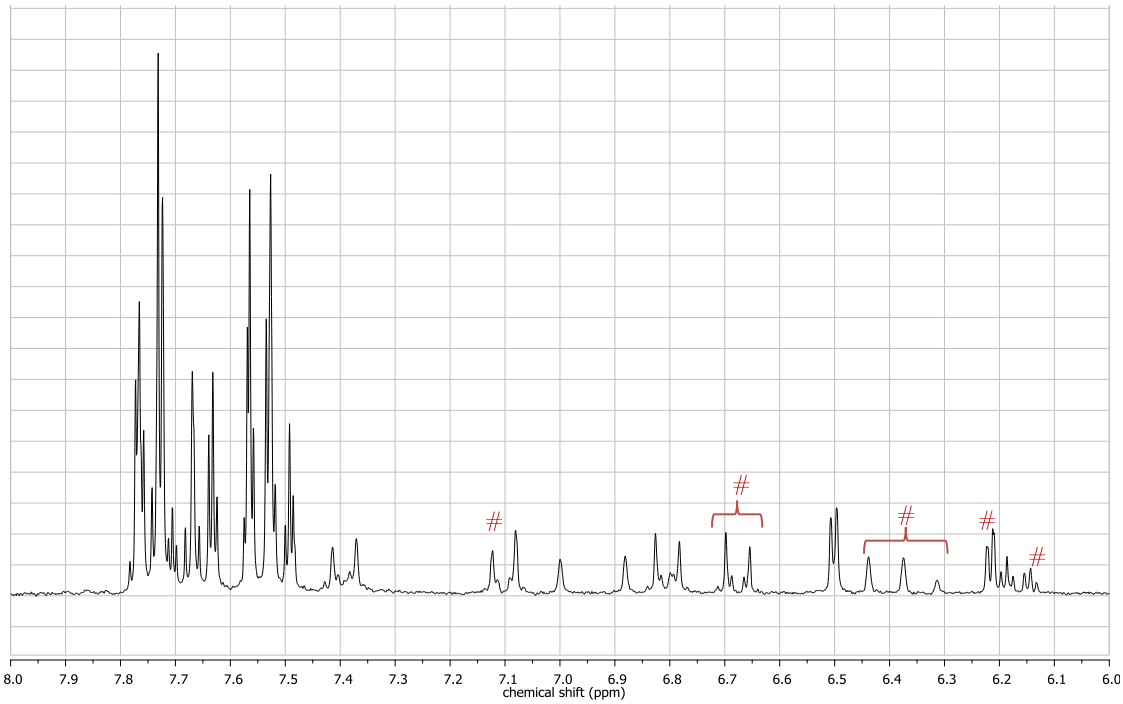

Figure 14 – Aromatic region of the 1H-NMR spectrum of resveratrol and benzophenone in a 1:1 CD3CN/D2O mixture, recorded after the CIDNP experiment was carried out; (#) corresponds to peaks assigned to the cis-isomer of resveratrol

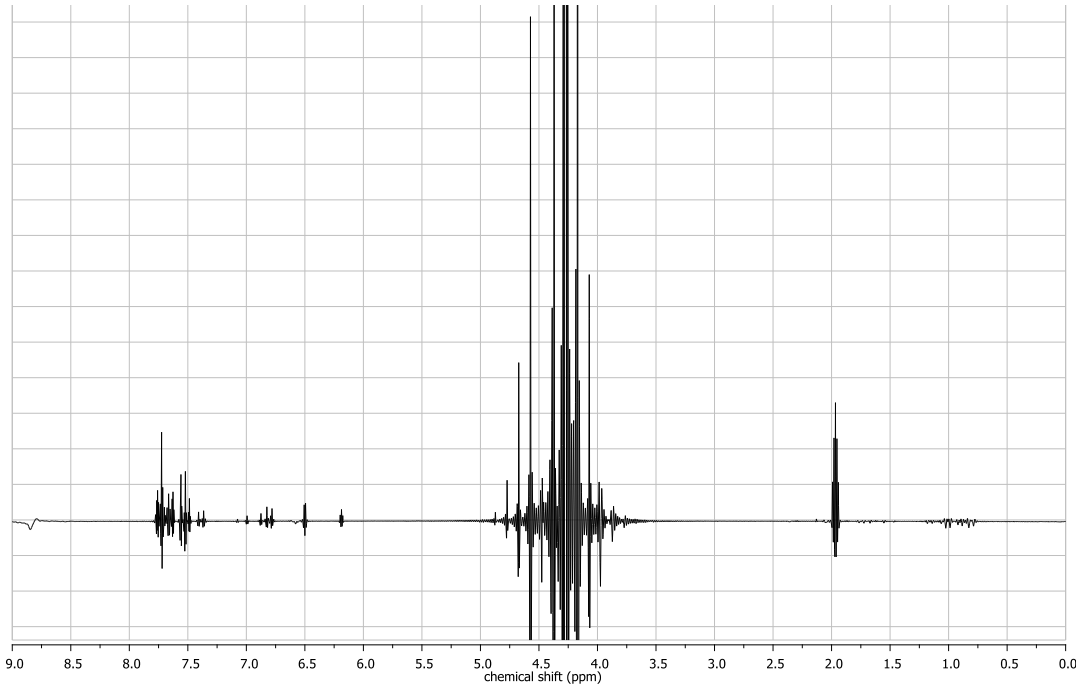

Figure 15 - ^{1}H-NMR spectrum of resveratrol and benzophenone recorded in a 1:1 CD3CN/H2O mixture; unusual peak shape is explained by the high H2O content resulting in over-modulation of the receiver

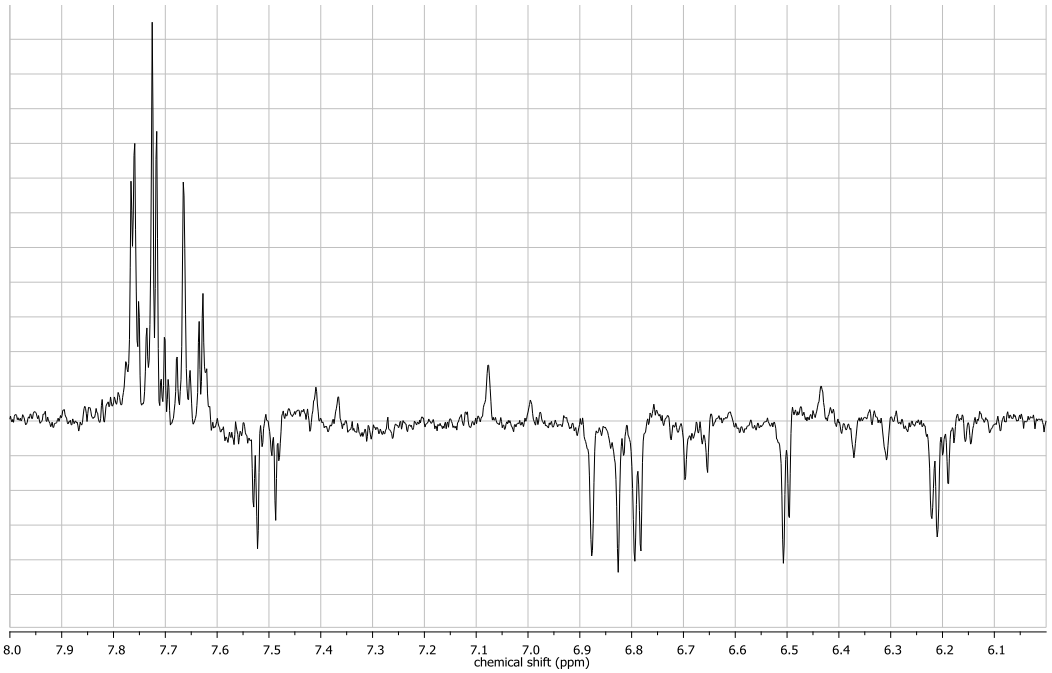

Figure 16 – Aromatic region of the ^{1}H-CIDNP spectrum of resveratrol and benzophenone recorded in a 1:1 CD3CN/H2O mixture

Interpretation of the CIDNP spectra can be accomplished by comparing the sign and the intensity of the polarized peaks with the results of DFT calculations.[73] As mentioned previously, the sign and the intensity of the signals can be correlated with the hyperfine coupling constants (hfc) of the formed radical. In Table 1, calculated hfc's of five selected species proposed in Scheme 3, are presented. Only five species were calculated as radicals $A^{-}B^{\bullet}$ and $A^{\bullet}B^{-}$ cannot be distinguished by DFT calculations. Therefore the two species are represented by $AB^{\bullet -}$. In order to allow better comparability with experimental results, all hfc are normalized to the largest value. The actual calculated values are given in the supplementary information. For symmetry equivalent protons, the mean value of the individual calculated hfc's is tabulated.

In Table 2, the intensities of the polarized peaks of the CIDNP spectrum stemming from resveratrol are tabulated, again normalized to the signal of highest intensity. From the results it can be stated that the polarization pattern preferentially fits to the hfc's of radical A•. This is in accordance with previous studies suggesting that this species is the thermodynamically most stable radical of resveratrol.

Table 1 – hfc of the possible radical species of resveratrol computed using DFT calculations; normalized to the signal of highest intensity

Proton / Species	2	4	6	7	8	10	11	13	14
	hfc [mT]								
A•	0,426	0,332	0,332	1,000	-0,329	-0,174	0,555	0,555	-0,174
B•	1,000	0,803	0,803	0,217	-0,053	0,008	-0,003	-0,003	0,008
$AB^{\bullet+}$	0,815	0,463	0,463	1,000	0,293	0,284	0,072	0,072	0,284
$AB^{\bullet-}$	0,686	0,375	0,375	1,000	-0,207	-0,111	0,508	0,508	-0,111
$BB^{\bullet-}$	0,125	1,000	1,000	0,183	-0,149	-0,042	0,017	0,017	-0,042

DFT calculations and experimental data do not align perfectly: The high polarization on hydrogen 2 is best represented by the calculation of B•. Possible, a mixture of both radical species is formed in the CIDNP experiment, yielding a polarization pattern partly corresponding to both species.

The calculated values for the polarization pattern of $AB^{\bullet-}$ are in good agreement with experimental data. Also it is notable that the calculated hfc's for A• and $AB^{\bullet-}$ are very similar.

Table 2 - Intensities of polarized peaks of resveratrol + benzophenone in CD3CN/D2O; normalized to the peak of highest intensity

Proton / Solvent	2	4	6	7	8	10	11	13	14
	hfc [mT]								
CH_3CN/D_2O	1,000	0,321	0,321	0,741	-0,444	-0,087	0,577	0,577	-0,087
CH_3CN/H_2O	1,000	0,310	0,310	0,980	-0,244	-0,062	0,614	0,614	-0,062

5.1.2. Resveratrol in the presence of anthraquinone

For the mixture of resveratrol and anthraquinone (AQ), ^{1}H NMR and ^{1}H CIDNP were recorded in binary mixtures of CD_3CN/D_2O and CD_3CN/H_2O. In the following, the CIDNP spectra are shown. The corresponding NMR spectra are presented in the supplementary information. Comparing the polarization pattern and the intensities of resveratrol to those recorded in the presence of benzophenone, it is obvious that both the

patterns and the relative intensities are essentially identical. Differences are detectable when comparing the polarization of resveratrol relative to the polarization of the photosensitizer: In the presence of benzophenone, resveratrol shows much less polarization than the photosensitizers. In the presence of anthraquinone, resveratrol displays much higher polarization then the photosensitizer as AQ is virtually not visible in the CIDNP spectrum.

The fact that AQ is almost not visible in the CIDNP spectrum can be explained by its poor solubility in the solvent mixture. This rationalization is in line with weak signals of AQ in ^{1}H NMR spectra. Moreover, after the series of experiments was performed, residual AQ was visible inside the NMR tube. Despite the poor solubility of AQ, polarized signals stemming from resveratrol are clearly visible in the CIDNP spectrum, suggesting that the HAT or electron transfer reaction from resveratrol to the triplet state of AQ still occurs.

Table 3 - Intensities of polarized peaks of resveratrol + anthraquinone in CD3CN/H2O; normalized to the peak of highest intensity

Proton / Solvent	2	4	6	7	8	10	11	13	14
					hfc [mT]				
CH_3CN/D_2O	-0,719	0,171	0,171	1,000	0,910	0,251	0,555	0,555	0,251
CH_3CN/H_2O	-0,401	0,024	0,024	1,000	-0,272	-0,052	0,807	0,807	-0,052

When analyzing the experimental data, it arises that the measured hfc's do not correlate with any of the calculated radical species. The main reason for these results can be rationalized by the poor solubility of AQ: only a small quantity of the photosensitizer was dissolved in the solvent. These small quantities of dissolved AQ are most likely not sufficient to produce a CIDNP spectrum which is suitable for an interpretation with respect to the formed radical species. Still, it can be stated that a radical species of resveratrol is formed within this experiment. Also, the triplet state of AQ seems to be highly reactive towards resveratrol, as the polyphenol exhibits detectable polarization whilst signals of the photosensitizer are absent in the CIDNP spectrum. Also it might be assumed that the solvent has a bigger impact on this reaction mixture than on the benzophenone/resveratrol system as the differences between the spectra recorded in

CD_3CN/D_2O and CD_3CN/H_2O are much more pronounced. Yet, this has to be viewed with caution due to the problems arising from the poor solubility of AQ.

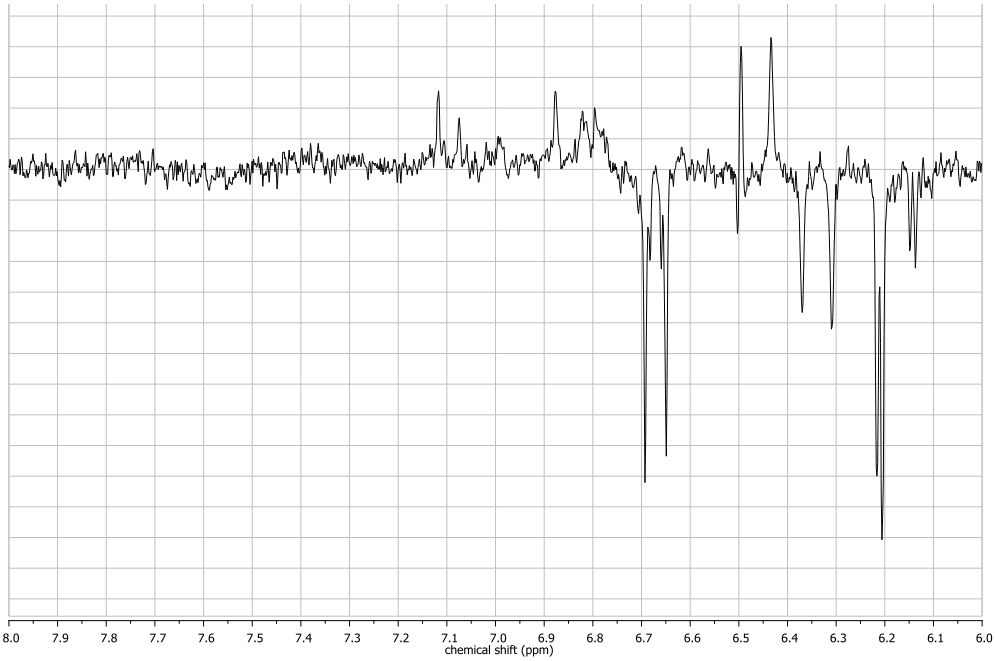

Figure 17 – Aromatic region of the ^{1}H-CIDNP spectrum of resveratrol and anthraquinone recorded in a 1:1 CD3CN/D2O mixture

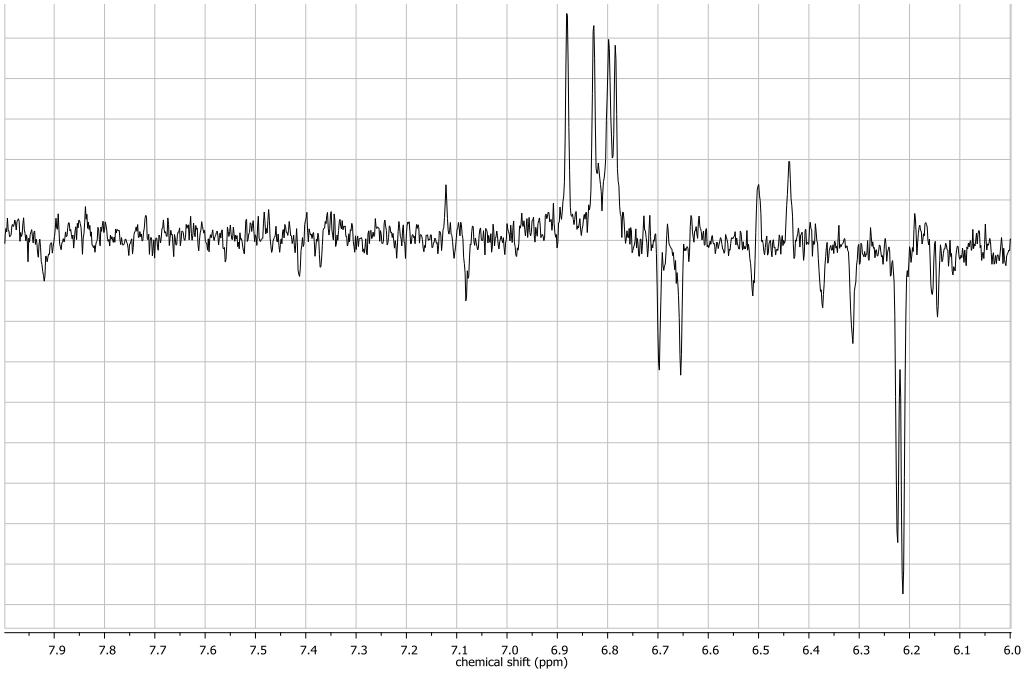

Figure 18 – Aromatic region of the ^{1}H-CIDNP spectrum of resveratrol and anthraquinone recorded in a 1:1 CD3CN/H2O mixture

5.1.3. Resveratrol in the presence of anthraquinone-1,5-disulfonic acid

^{1}H NMR as well as ^{1}H CIDNP experiments of resveratrol in the presence of AQDS have been performed in binary mixtures of CD_3CN/D_2O and CD_3CN/H_2O yielding the spectra shown in the following figures and in the supplementary information.

Comparing the spectra recorded in the two different solvent mixtures, only minor differences are detected. The polarization pattern and the intensities of the signals in the reaction mixtures also show no substantial differences when compared with the spectra recorded for the resveratrol/benzophenone system.

Table 4 - Intensities of polarized peaks of resveratrol + anthraquinone – 1, 5 – disulfonic acid in CD3CN/H2O; normalized to the peak of highest intensity

Proton / Solvent	2	4	6	7	8	10	11	13	14
	hfc [mT]								
CH_3CN/D_2O	-0,342	0,298	0,298	1,000	-0,711	-0,439	0,544	0,544	-0,439
CH_3CN/H_2O	-0,139	0,109	0,109	1,000	-0,948	-0,435	0,517	0,517	-0,435

For this reaction system, the experimental data again suggests either the formation of the species A• or $AB^{-\bullet}$. The signals recorded in CH_3CN/D_2O and CH_3CN/H_2O do not exhibit any significant differences. These results underline the conclusion already drawn from the resveratrol/benzophenone system as they suggest the formation of the same radical species from resveratrol.

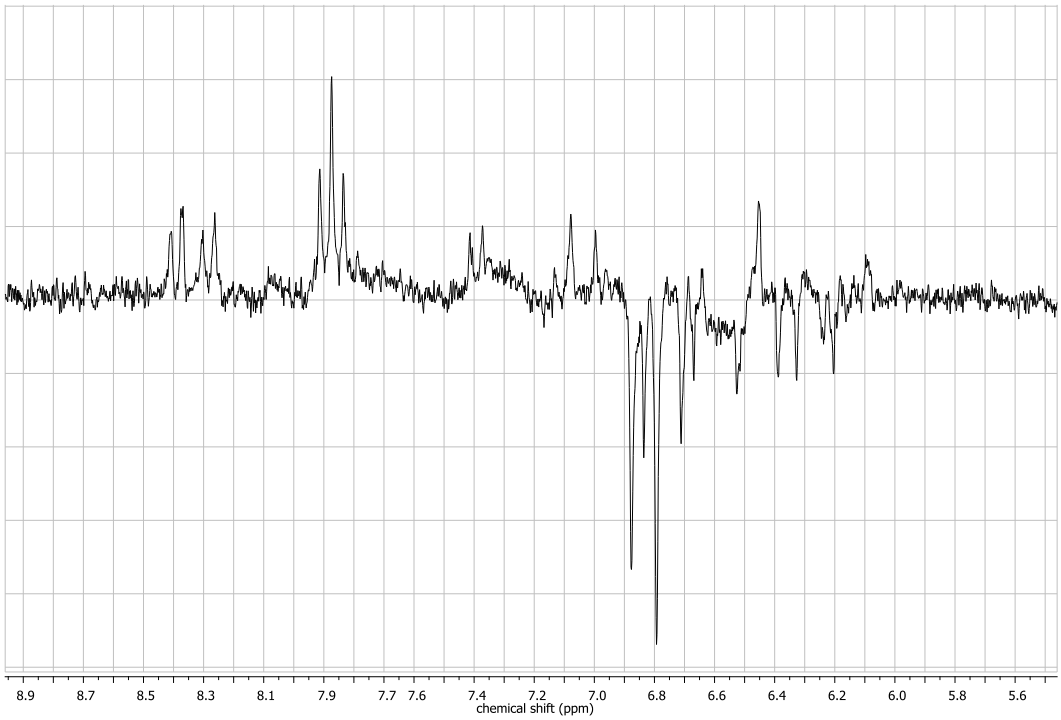

Figure 19 – Aromatic region of the ^{1}H-CIDNP spectrum of resveratrol and anthraquinone - 1, 5 – disulfonic acid recorded in a 1:1 CD3CN/D2O mixture

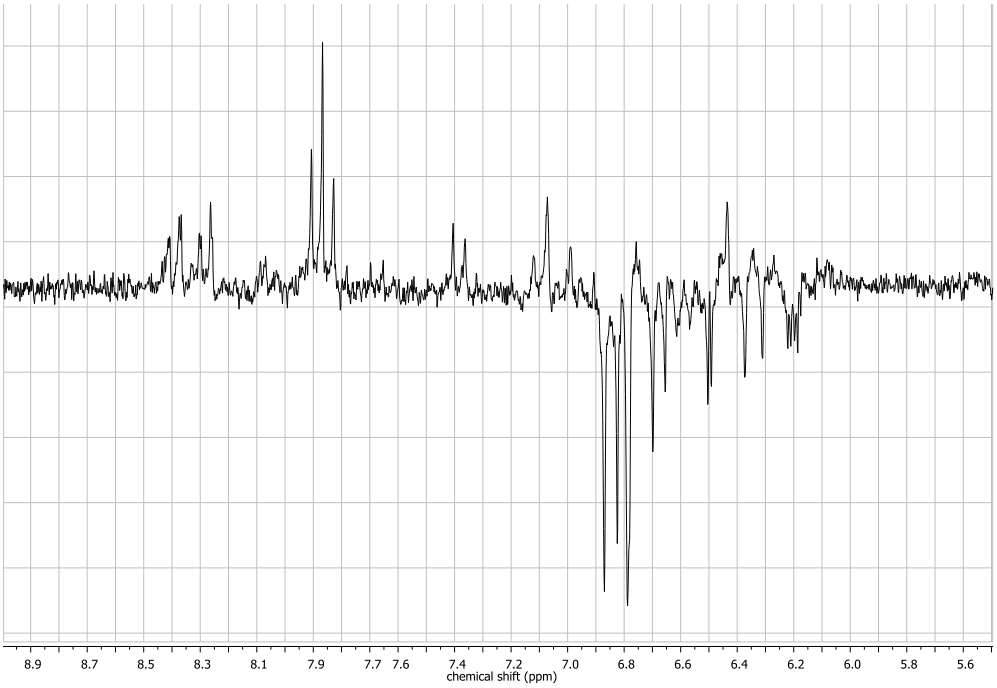

Figure 20 – Aromatic region of the ^{1}H-CIDNP spectrum of resveratrol and anthraquinone - 1, 5 – disulfonic acid recorded in a 1:1 CD3CN/H2O mixture

5.1.4. Resveratrol in presence of benzophenone at different pH-Values

^{1}H NMR spectra as well as ^{1}H CIDNP spectra of resveratrol in the presence of benzophenone in CD_3CN/D_2O at different pH-values ranging from 0.64 to 13.64 were recorded. The exact pH values of 0.64, 2.45, 9.72 and 13.46 were achieved by adding sulfuric acid-d^2, acidic acid-d^4, pyridine-d^6 and sodium hydroxide-d^1 to the reaction mixture, respectively. Deuterated acids and bases were chosen over their non-deuterated counterparts to avoid undesired signals in the ^{1}H NMR experiments. The reaction mixture of resveratrol and benzophenone in this binary solvent mixture (without the addition of any further compounds described above) corresponds to a pH value of 6.65. The small shifts of the signal are attributed to minor differences in the composition of the solvent mixtures leading to differences in the lock of the sample inside the NMR spectrometer.

It is easily recognized that there is no difference in polarization in the pH range from 2.45 to 9.72, meaning that there is no change in the antioxidant activity of resveratrol in this pH-range. Differences only occur when going to both very acidic and very basic conditions. At very acidic conditions, no polarization of resveratrol is observed, even though there still is polarization on the benzophenone. Also, a new polarized signals at around 5.5 ppm appears in the spectrum. Most likely this polarization is due to hydrogen abstraction of the benzophenone triplet from the added acid as can be seen from the ^{1}H NMR spectra (see supplementary information).

At very basic conditions, no polarization at all is observed in the recorded CIDNP spectrum. This complete absence of signals is explained by the fact that at this pH range, all three hydroxyl groups of resveratrol are deprotonated - the pKa-values of the phenolic hydroxyl groups are 8.8, 9.8 and 11.4[74] - rendering it useless in terms of antioxidant activity at high pH values.

Even though these studies clearly show restrictions for the antioxidant activity of resveratrol at both very high and very low pH values, one has to be aware that these conditions are far away from physiological pH. Within the pH range that can occur in biological systems it is shown that the mechanism inducing the antioxidant activity of resveratrol does not seem to change.

When considering the pKa-values of 8.8, 9.8 and 11.4 for the phenolic OH groups of resveratrol it can be expected that at neutral pH, the fully protonated and the mono-deprotonated as well as small quantities of the di-deprotonated species are present. This means at neutral pH, both HAT and a concerted electron-proton transfer (EPT) are possible reaction mechanisms forming the species $A^{\bullet}$ and $AB^{-\bullet}$, respectively. At low pH values, resveratrol is present almost exclusively as the fully protonated species making HAT the dominating process for the reaction with the triplet state of the photosensitizer. At higher pH, correspondingly, the formation of the radical anion should be more favored as resveratrol is present mainly as the mono- and di-deprotonated species, making a concerted electron-proton transfer (EPT) the dominating reaction mechanism.

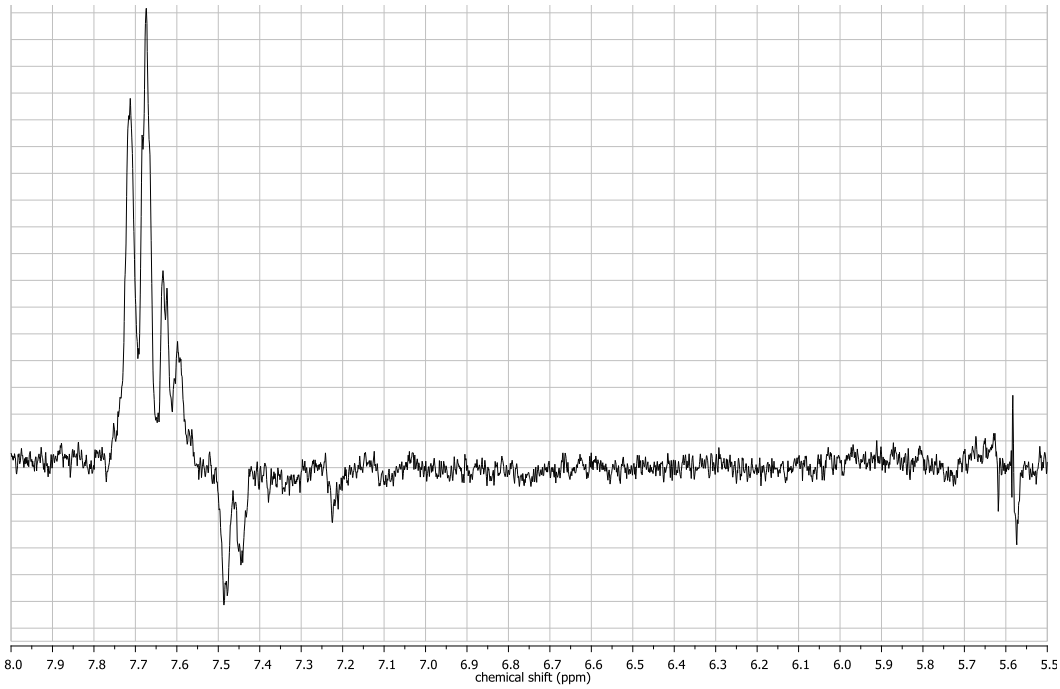

Figure 21 - Aromatic region of the ^{1}H-CIDNP spectrum of resveratrol and benzophenone recorded in CD3CN/D2O 1:1; pH = 0.64

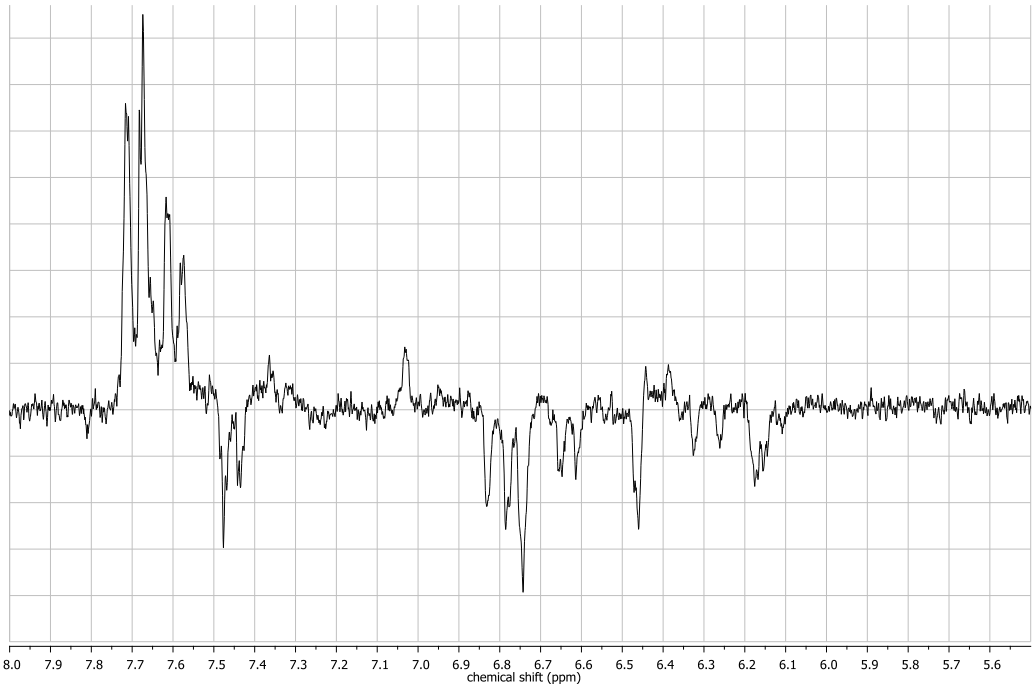

Figure 22 - Aromatic region of the ^{1}H-CIDNP spectrum of resveratrol and benzophenone recorded in CD3CN/D2O 1:1; pH = 2.45

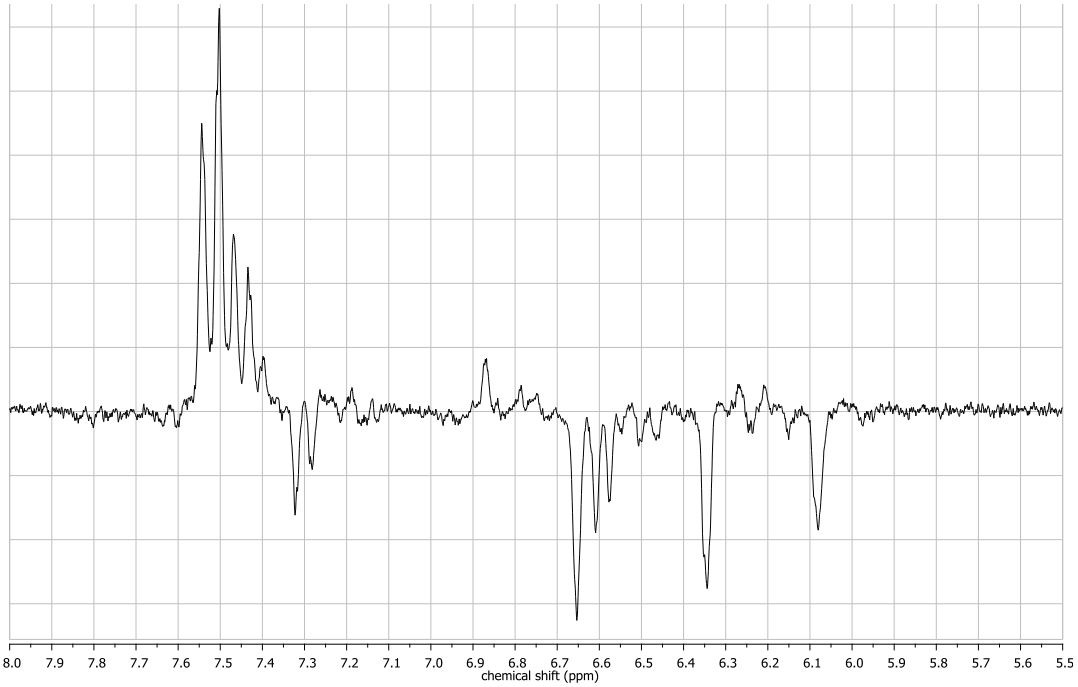

Figure 23 - Aromatic region of the ^{1}H-CIDNP spectrum of resveratrol and benzophenone recorded in CD3CN/D2O 1:1; pH = 9.72

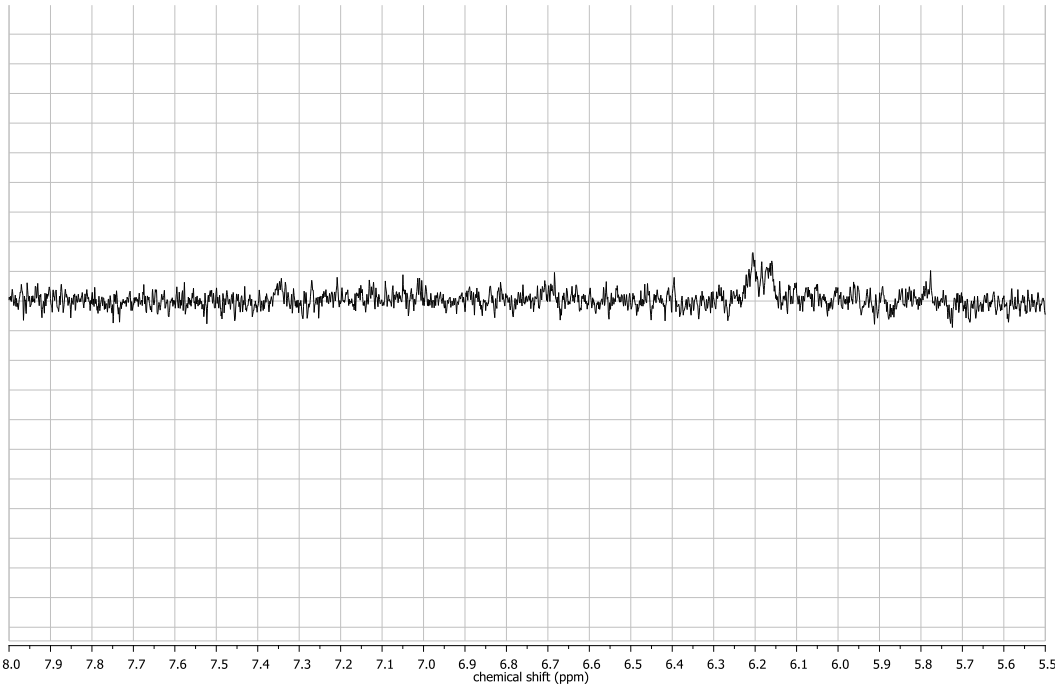

Figure 24 - aromatic region of the ^{1}H-CIDNP spectrum of resveratrol and benzophenone recorded in CD_3CN/D_2O 1:1; pH = 13.46

5.2 EPR measurements

5.2.1. Resveratrol in the presence of different photosensitizers

EPR measurements of resveratrol in the presence of either one of the photosensitizers BP, AQ, AQDS or AQDS-2,6 were performed in 1:1 binary mixtures of CH_3CN/H_2O. The experimental setup and parameters are described in Chapter 4.3. Typical concentrations were 15 mM for resveratrol and 60 mM for the photosensitizers.

The EPR spectra of resveratrol recorded in the presence of either BP or AQ did not yield any signals indicating the formation of radicals. There are several reasons for this behavior: in CIDNP, polarization can be built up in the nanosecond time regime.[75] Information on the polarization is then 'stored' within the diamagnetic products giving rise to information about very fast processes. The detection limit in EPR is also in the nanosecond time scale. However, in EPR, radical species are probed directly, therefore a sufficient steady-state concentration of radicals is required to observe signals. In the case of the resveratrol/AQ and resveratrol/BP systems, it is possible that the reaction rate for

the formation of diamagnetic products from the radicals *(k_p)* is higher than the reaction rate for the formation of the radicals itself *(k_r)*. This eventually results in a steady-state concentration of radicals which is too low to be detected with the employed experimental setup. Also, one factor which could play a role are the different active volumes in CIDNP and EPR – in CIDNP the active volume is approximately five times higher than in EPR giving rise to a larger total amount of radicals.

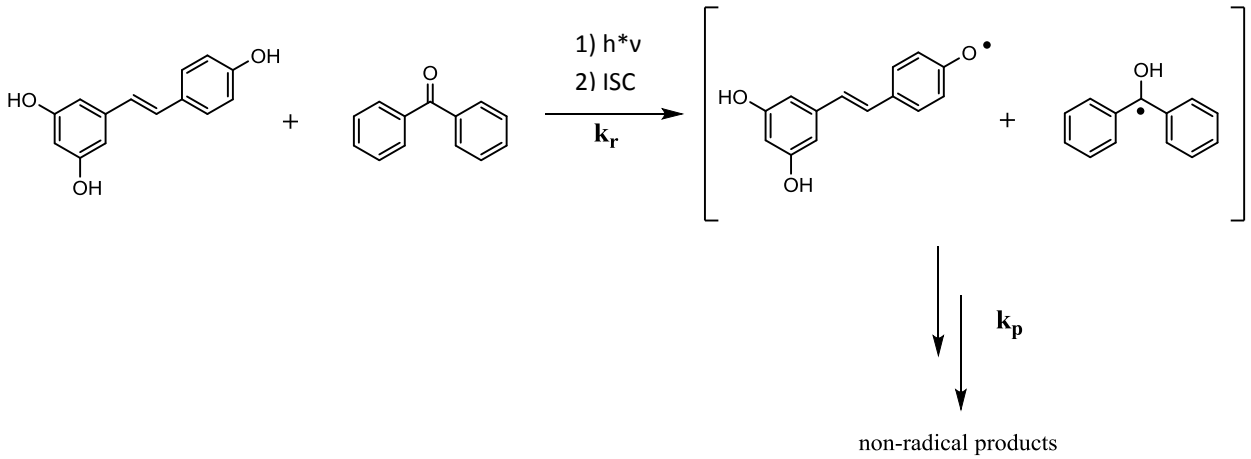

Scheme 7 - HAT from resveratrol to the triplet state of BP and follow-up reactions

When using AQDS and AQDS-2,6 however, EPR spectra are detected (Figures 26 - 28) This can possibly be explained by a higher steady-state concentration of radicals arising from a smaller ratio k_p/k_r. It also has to be kept in mind that the steady state concentration in the EPR experiments depends on the utilized flow rate.

The spectra shown in Figure 26 and 27 correspond to a radical stemming from AQDS-2,6. In Figure 26 the simulation for the radical anion is shown, while the simulation in Figure 27 uses the data for a neutral radical of AQDS-2,6. Neither one of the two simulations correlates entirely to the experimental data. It is also notable that both simulations are fairly similar. If the radical anion of AQDS-2,6 is the main species formed this would mean that resveratrol reacts via an electron transfer with the triplet state of the photosensitizer. If the main species is the neutral radical, HAT is the dominant reaction pathway of resveratrol with the AQDS-2,6 triplet.

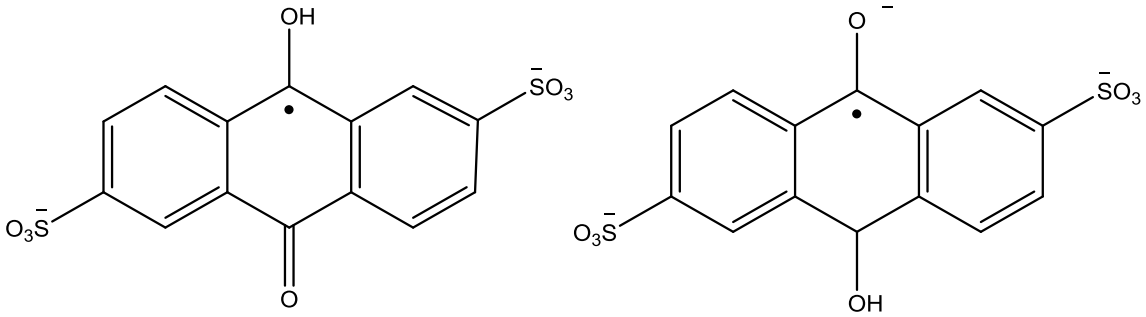

Figure 25 - Structure of the radicals AQDS• (left) and AQDS•- (right)

Table 5 - hfc's of the radicals AQDS• and AQDS•- used for spectra simulation

Radical	hfc's [mT]
AQDS•-	a(2H) = 1.20[76]
	a(2H) = 0.41[76]
	a(2H) = 0.36[76]
AQDS•	a(2H) = 1.20[76]
	a(2H) = 0.61[76]

As the simulation does not align perfectly with experimental data, it can be assumed that the spectrum is produced by the overlap of signals from the neutral radical and the radical anion. This is good agreement with results obtained from CIDNP spectroscopy. CIDNP suggests both HAT and EPT as possible reaction mechanisms for the reaction of resveratrol with the photosensitizer triplet state. HAT would lead to a neutral radical of AQDS-2,6, whilst the electron transfer process of EPT would give rise to the radical anion of AQDS-2,6. As no signals corresponding to a radical species of resveratrol are present in the EPR spectra, no statement about the initial reaction pathway defining the antioxidant activity of the polyphenol can made with certainty from the EPR spectra.

The spectrum shown in Figure 28 could not be interpreted yet. It is highly likely that it also corresponds to a radical species of the photosensitizer – in this case AQDS. The possibility that this spectrum corresponds to any radical species of resveratrol can be ruled out: an identical spectrum was obtained repeating the experiment was repeated with AQDS in the presence of catechol.

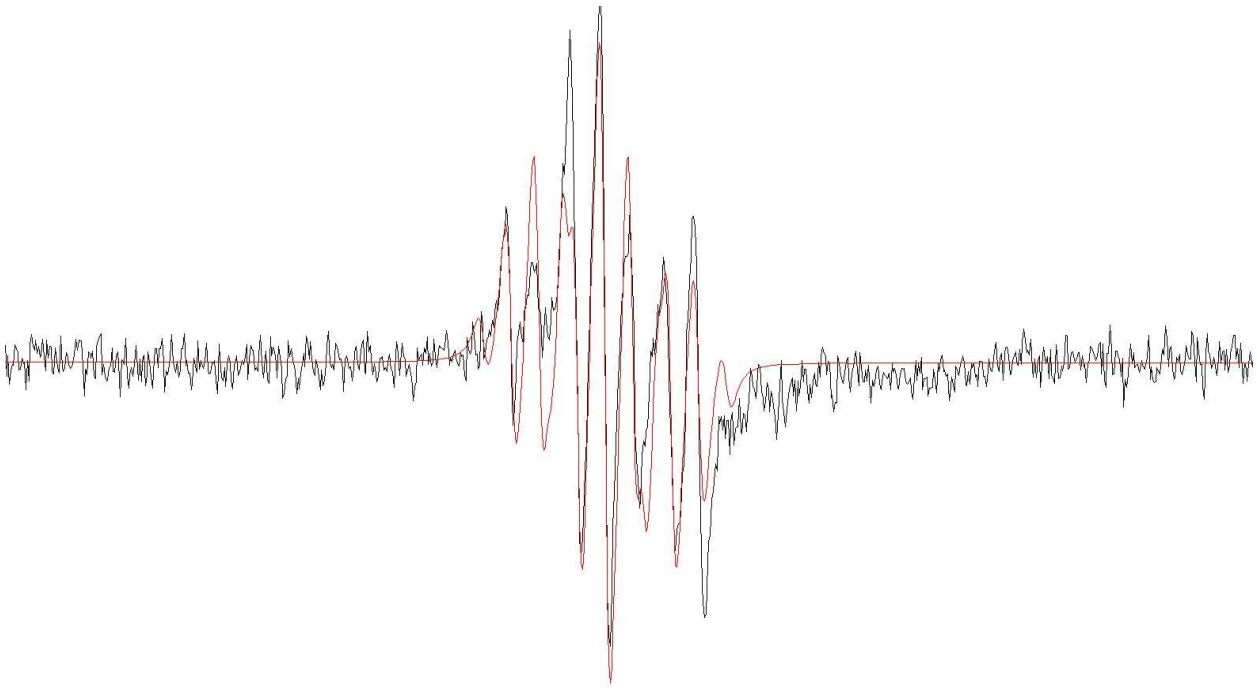

Figure 26 – EPR spectrum of a solution of resveratrol and AQDS-2,6 in CH_3CN/H_2O upon continuous irradiation (black) and the simulation using literature values for the neutral radical of AQDS-2,6 (red)

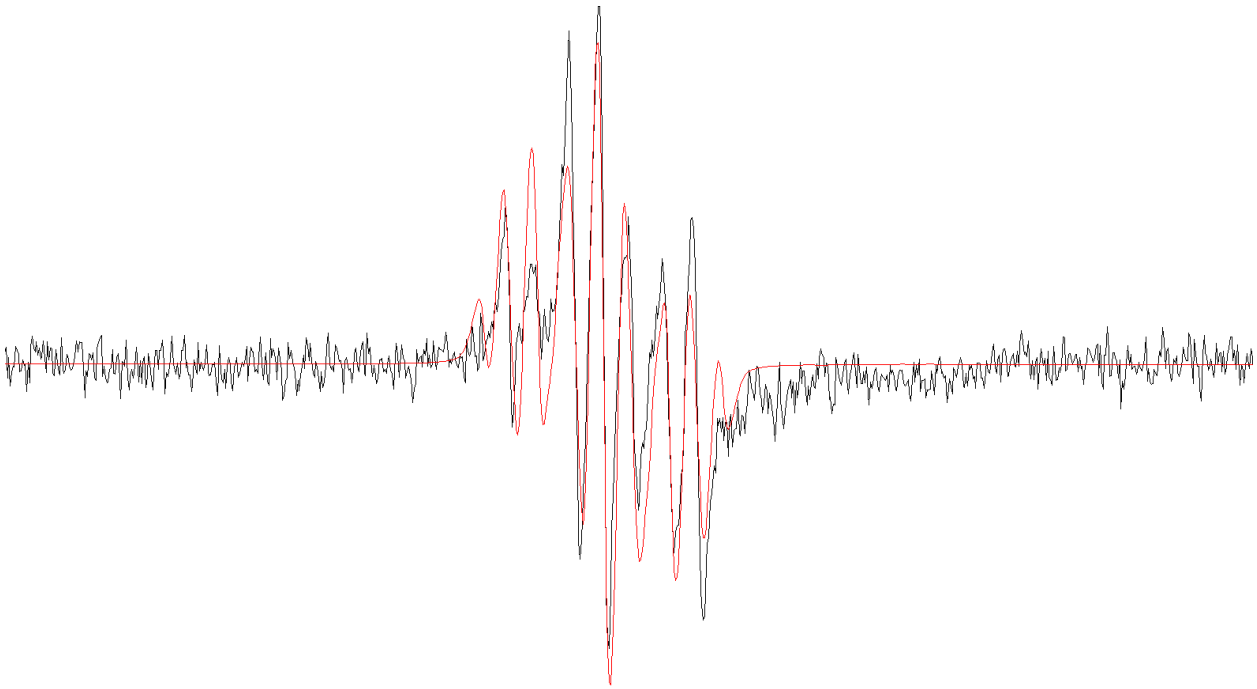

Figure 27 -– EPR spectrum of a solution of resveratrol and AQDS-2,6 in CH_3CN/H_2O upon continuous irradiation (black) and the simulation using literature values for the radical anion of AQDS-2,6 (red)

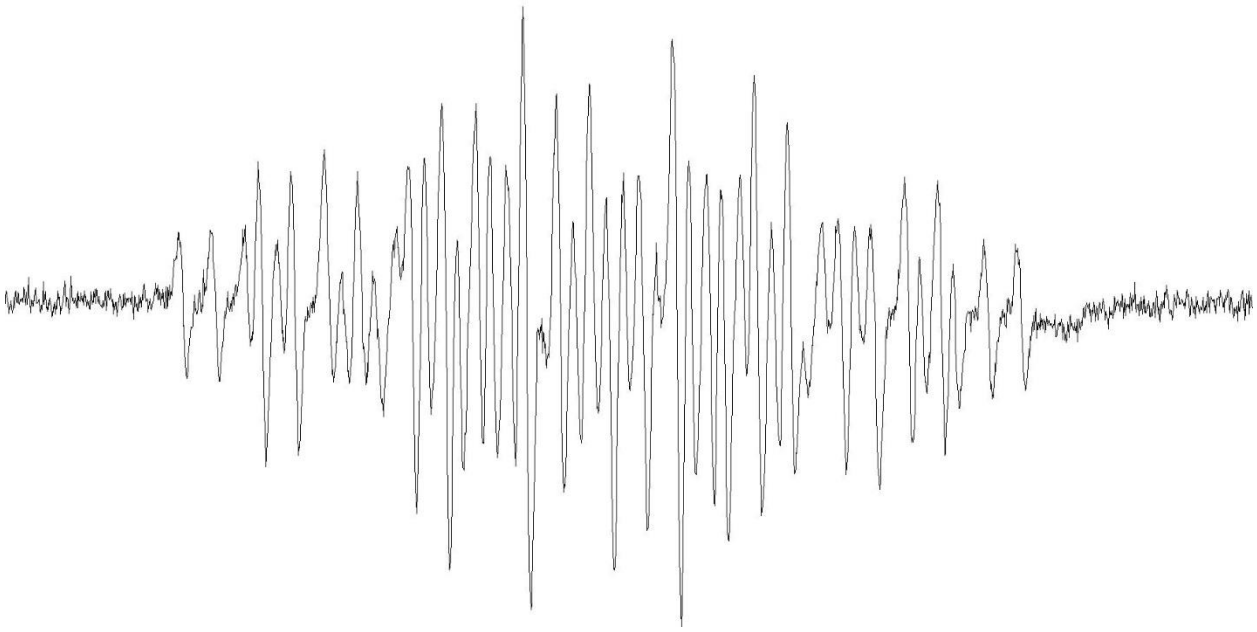

Figure 28 - EPR spectrum of a solution of resveratrol and AQDS in CH_3CN/H_2O upon continuous irradiation

5.2.2. Resveratrol in the presence of Fenton's reagent

Fenton's reagent was used to generate hydroxyl radicals directly using a flat cell placed inside the cavitiy of the EPR spectrometer. The setup consisted of a syringe pump mounted with three syringes containing H_2O_2 (30% in H_2O), a mixture of iron(II) sulfate (10 mM) and disodium ethylenediamine tetraacidic acid (Na_2EDTA; 10 mM) for the stabilization of the Fe^{2+} ion in H_2O, and a solution of resveratrol in acetronitile (15 mM). The mixing of the solutions was realized by combining three tubes directly in front of the flat cell.

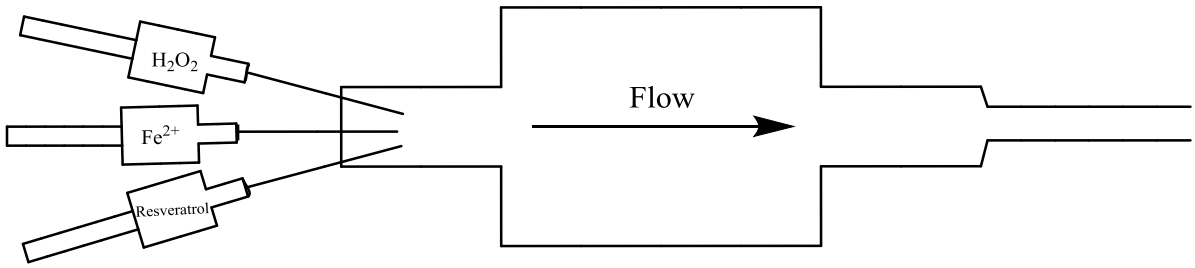

Scheme 8 - Experimental setup for Fenton EPR experiments

Unfortunatly, this set up did not lead to the detection of EPR signals. Only a color change of the solution from yellow to red owing to the oxidation of Fe^{2+} to Fe^{3+} in the presence of H_2O_2 indicated that a reaction took place. The absence of the EPR signals does not imply that there is no chemical reaction besides the oxidation of iron: According to equation (8) shown in chapter 2.3, when Fe^{2+} is oxidized to Fe^{3+} by hydrogen peroxide, a hydroxyl radical is formed. Since these radicals show high and unselective reactivity towards almost any given substrate it is unlikely that no reaction of $\bullet$OH and resveratrol is occuring. A possible explanation for the absence of any peaks lies in the fact that it was not possible to tune the spectrometer with the employed experimental setup.

5.2.3. Resveratrol in the presence of photo-Fenton reagents

EPR measurements of resveratrol in the presence of N-HPT as the photo-Fenton reagent were carried out using the same experimental conditions described in chapter 5.2.1. The concentration of the hydroxyl radical generator was 15 mM. The concentration of resveratrol was 15 mM.

Again, however, no EPR could be detected. One explanation is the fact that N-HPT exhibits a tautomerization to the thiophenol,[50] therefore reducing the ability of $\bullet$OH generation. Again, this can possibly be explained by a low steady-state concentration of radicals inside the cavity of the EPR spectrometer due to fast follow up-reactions of the radicals to non-radical products or due to an insufficient flow rate for the employed experimental setup.

5.3 CIDEP measurements

CIDEP measurements of resveratrol in the presence of the photosensitizers BP, AQ and AQDS were carried out in 1:1 binary mixture of CH_3CN/H_2O. The experimental setup and parameters are described in Chapter 4.4. Typical concentrations were 15 mM for resveratrol and 60 mM for the photosensitizers.

None of the different photosensitizer/resveratrol combinations exhibits a detectable CIDEP polarization. In this case, this behavior cannot be explained by low steady-state concentration of radicals, as in CIDEP (like in CIDNP) polarization is detected. Likely, the fact that – other than in CIDNP - no polarization of the resveratrol/photosensitizer systems is observed in CIDEP stems from the different time-scales of the two techniques: in CIDNP, the polarization is 'stored' in the diamagnetic products, allowing the detection of species formed on the (sub-)nanosecond timescale. In CIDEP, however, the detection is limited by the dead-time of the spectrometer[77] – which in this case is 50 ns. This means that radicals, which have a shorter lifetime than 50 ns cannot be detected in CIDEP while they still give rise to polarization in CIDNP. This is likely the case for the investigated resveratrol/photosensitizer systems, implying a very short lifetime of the primary resveratrol radicals.

6 Summary and Conclusion

The antioxidant activity of resveratrol can be explained either by EPT or HAT based on the results of CIDNP spectroscopy. However, the neutral radical A• and the radical anion $AB^{-\bullet}$ are not sufficiently distinguishable by CIDNP. Spectra recorded in the presence of different photosensitizers exhibit only minor differences. The experiments performed at different pH values suggest that both EPT and HAT are possible reaction pathways for resveratrol: at acidic conditions the formation of the neutral radical species should be more favored, as an additional deprotonation after hydrogen atom transfer is unlikely. In basic conditions this deprotonation step is more favored, making EPT the dominating reaction pathway. At neutral pH, most likely a combination of EPT and HAT is responsible for the antioxidant activity of resveratrol. This behavior is underlined by the pKa-values of the phenolic hydroxyl groups of 8.8, 9.8 and 11.4: These values indicate that at acidic conditions resveratrol is present as fully protonated species, while at basic conditions it is present as the mono- or di-deprotonated species. Accordingly, at neutral pH, both the fully protonated and the mono-deprotonated species are present.

The results obtained from EPR spectroscopy confirm the results obtained from CIDNP. The spectra recorded for the reaction of resveratrol with the triplet state of AQDS-2,6 suggest a combination of HAT and EPT. The spectra obtained for the resveratrol/AQDS system exhibit broad signals which, to this point, could not be assigned to a radical species. The EPR spectra of resveratrol in the presence of other photosensitizers did not yield any signals suggesting the formation of a radical species. This can be explained by low steady-state concentration arising from fast follow-up reactions of the formed radicals.

In CIDEP, the fact that no polarization was observed can be explained by a low lifetime (< 50 ns) of radicals formed from the resveratrol/photosensitizer system. Because of the dead-time of the spectrometer used, radicals with such low lifetime cannot be detected.

The antioxidant activity of resveratrol still represents an interesting scientific area. Previous studies suggest that the polyphenol resveratrol exhibits strong antioxidant activity as it is an effective quencher of ROS. However, to my knowledge, only little experimental data on the mechanistic behavior of this antioxidant activity is available.

The present work provides an insight to these reactions employing various experimental techniques. Most likely a combination of HAT and EPT is responsible for the function of resveratrol as an antioxidant. Also, the experimental data imply a short lifetime for the primary resveratrol radicals (< 50 ns) due to very fast follow up reactions.

7 Supplementary Information

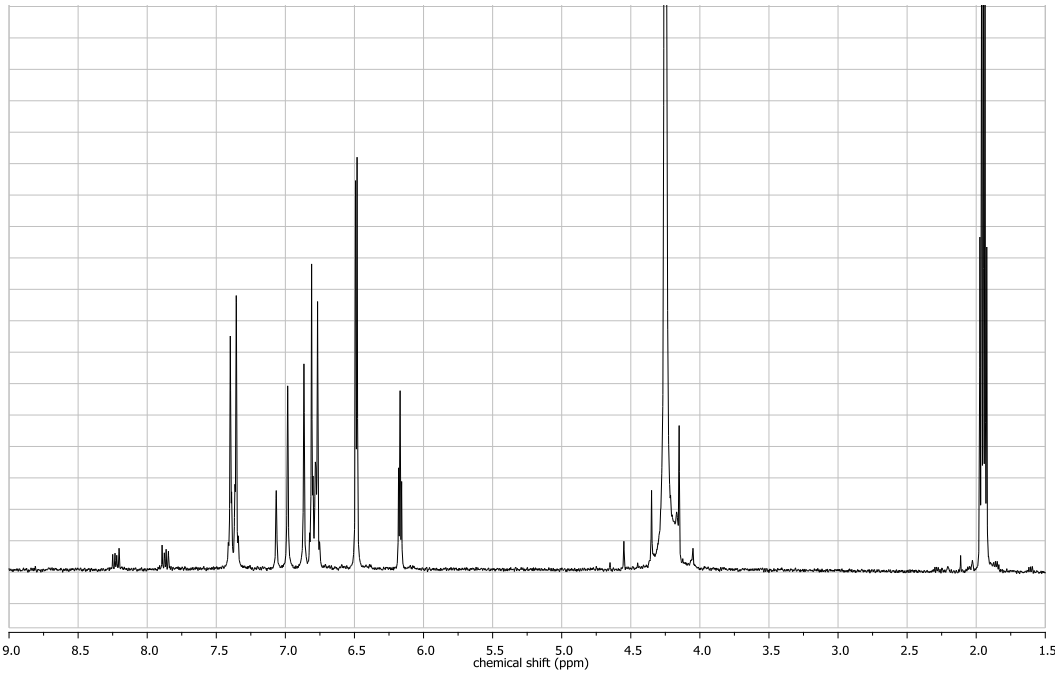

Figure 29 - 1H-NMR spectrum of resveratrol and AQ recorded in a 1:1 CD3CN/D2O mixture

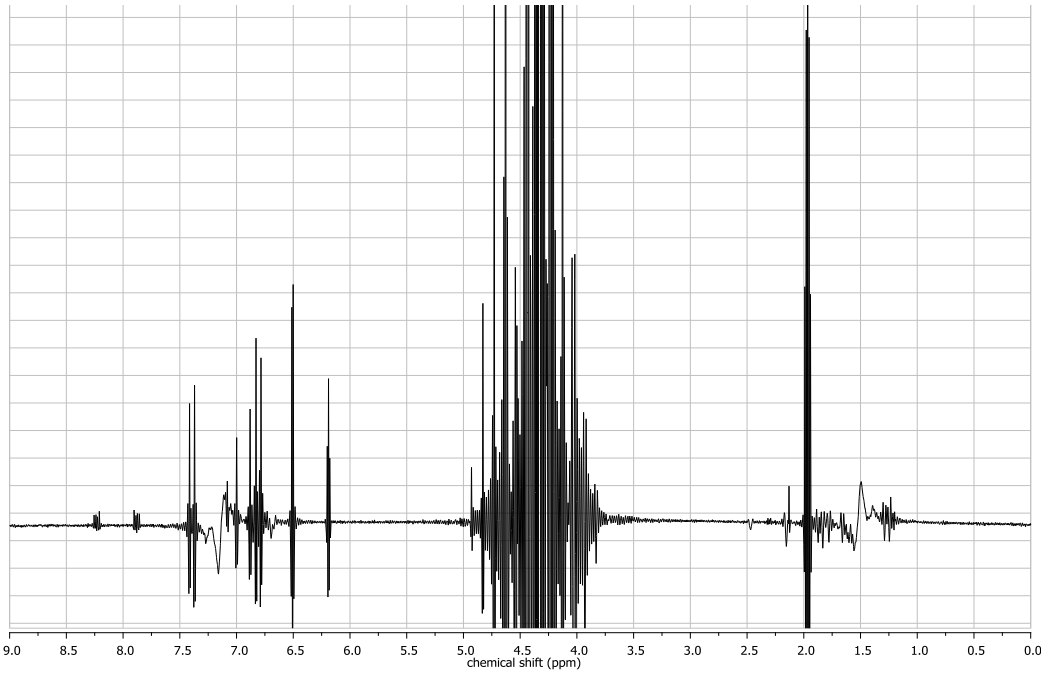

Figure 30 - 1H-NMR spectrum of resveratrol and AQ recorded in a 1:1 CD3CN/H2O mixture; unusual peak shape is explained by the high H2O content resulting in over-modulation of the receiver

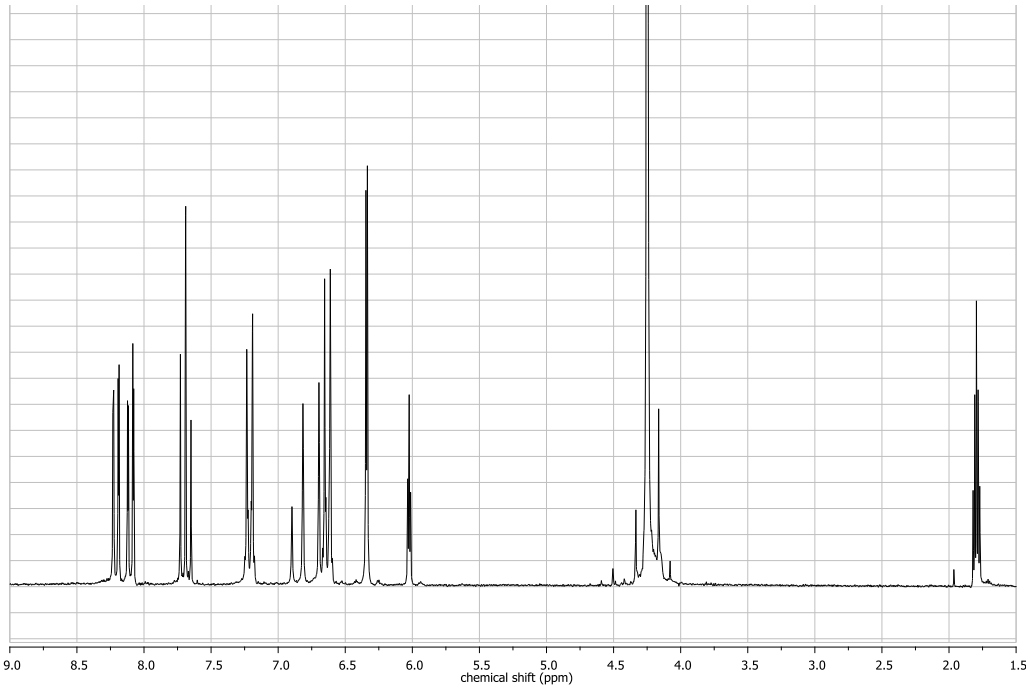

Figure 31 - 1H-NMR spectrum of resveratrol and AQDS recorded in a 1:1 CD3CN/D2O mixture

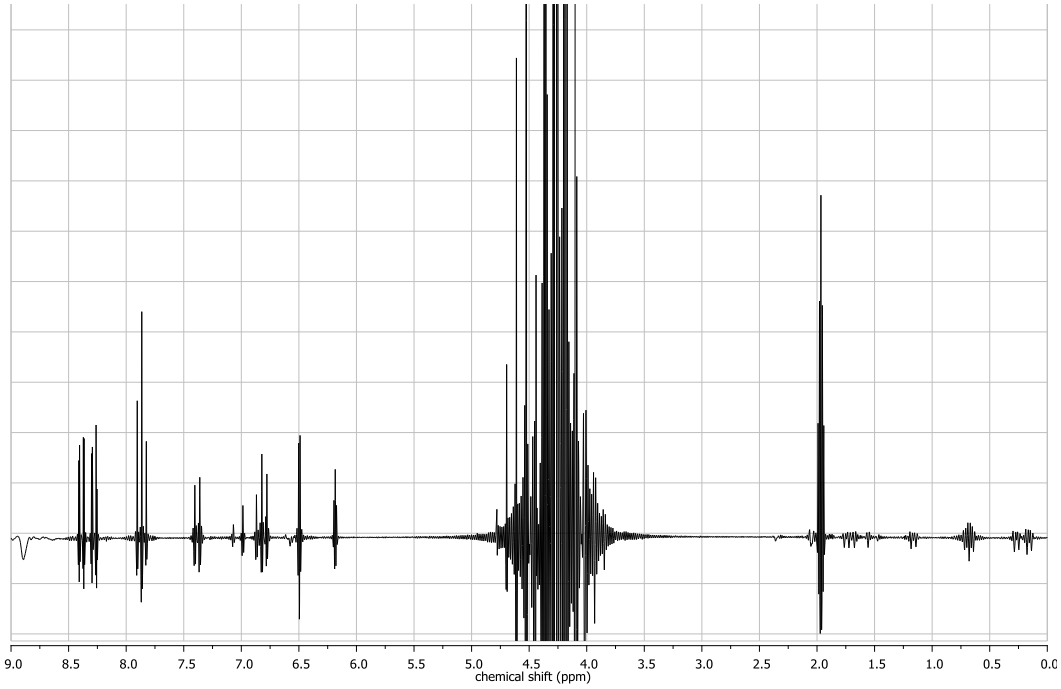

Figure 32 - 1H-NMR spectrum of resveratrol and AQDS recorded in a 1:1 CD3CN/H2O mixture; unusual peak shape is explained by the high H2O content resulting in over-modulation of the receiver

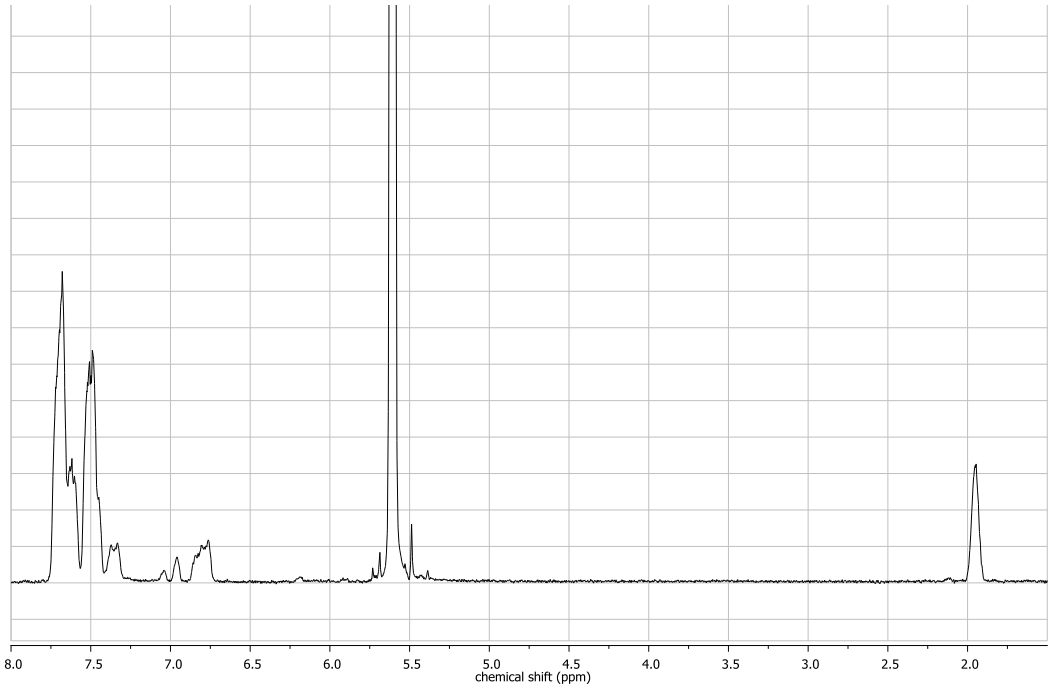

Figure 33 - 1H-NMR spectrum of resveratrol and BP recorded in a 1:1 CD3CN/D2O mixture; pH = 0.64

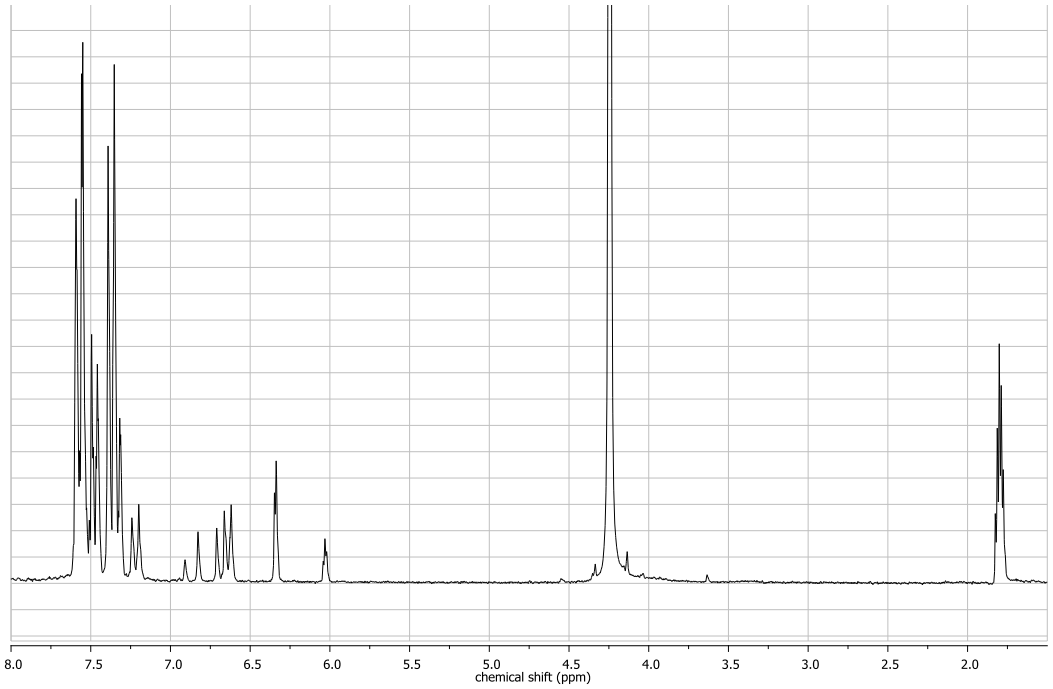

Figure 34 - 1H-NMR spectrum of resveratrol and BP recorded in a 1:1 CD3CN/D2O mixture; pH = 2.45

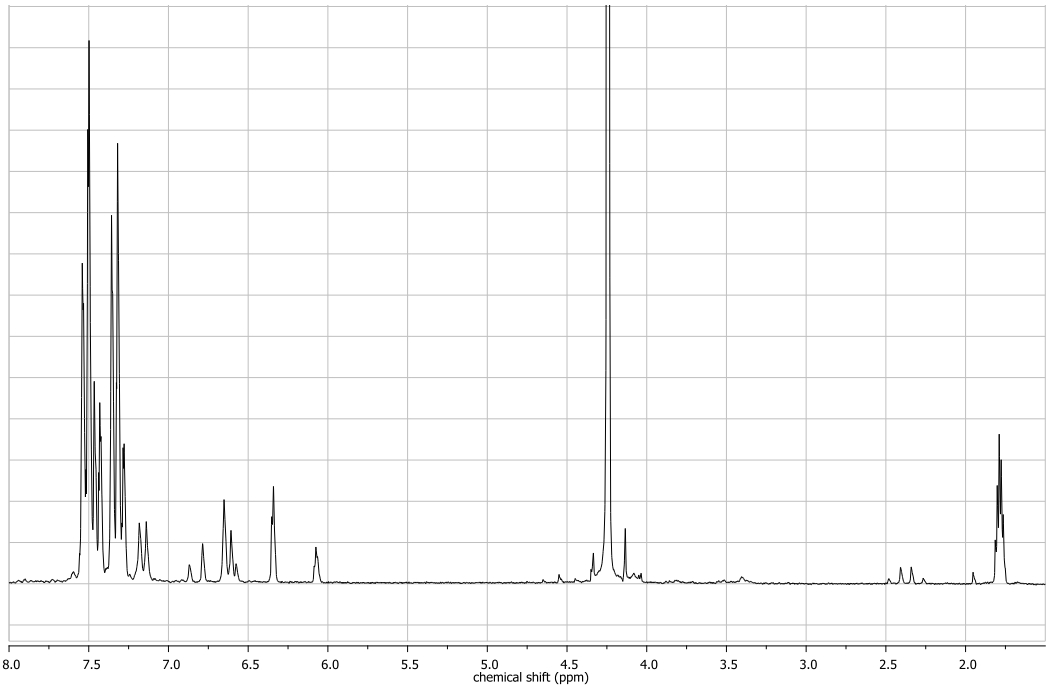

Figure 35 - 1H-NMR spectrum of resveratrol and BP recorded in a 1:1 CD3CN/D2O mixture; pH = 9.72

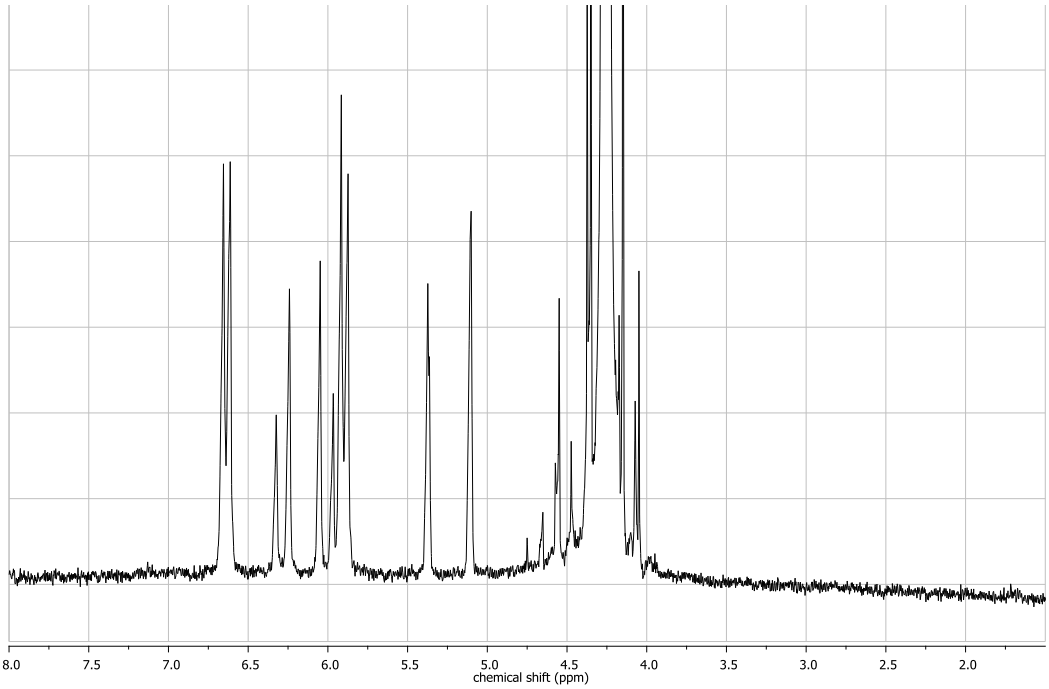

Figure 36 - 1H-NMR spectrum of resveratrol and BP recorded in a 1:1 CD3CN/D2O mixture; pH = 13,46

Table 6 - hfc of the possible radical species of resveratrol computed using DFT calculations

Proton / Species	2	4	6	7	8	10	11	13	14
	hfc [mT]								
A•	-7,337	-5,971	-5,481	-17,235	5,674	2,690	-8,805	-10,341	3,319
B•	-19,078	-7,158	-23,476	-4,131	1,009	-0,121	-0,043	0,162	-0,172
$AB^{\bullet+}$	-12,758	-6,131	-8,353	-15,648	-4,578	-4,152	-0,790	-1,476	-4,731
$AB^{\bullet-}$	-10,619	-3,561	-8,054	-15,484	3,205	1,998	-7,224	-8,521	1,440
$BB^{\bullet-}$	-3,170	-20,052	-30,547	-4,623	3,781	1,071	-0,374	-0,484	1,072

8 References

1. Li, B. & Pratt, D. A. Free Radical Biology and Medicine Methods for determining the efficacy of radical-trapping antioxidants. **82,** 187–202 (2015).
2. Re, R. *et al.* Antioxidant activity applying an improved ABTS radical cation decolorization assay. *Free Radic. Biol. Med.* **26,** 1231–1237 (1999).
3. Lago, J. *et al.* Structure-Activity Association of Flavonoids in Lung Diseases. *Molecules* **19,** 3570–3595 (2014).
4. Brito, O., Almeida, L. M. & Dinis, T. C. No Title. *Free Radic. Res. Commun.* **36,** 176 (2002).
5. Brede, O., Stajanovic, S. & Sprinz, H. No Title. *Free Radic. Res. Commun.* **36,** 76 (2002).
6. Wang, M., Li, J., Rangarajan, M., Shao, Y. & Lavoie, E. J. Antioxidative Phenolic Compounds from Sage (Salvia officinalis). 4869–4873 (1998).
7. Pietraforte, D., Turco, L., Azzini, E. & Minetti, M. On-line EPR study of free radicals induced by peroxidase / H 2 O 2 in human low-density lipoprotein. **1583,** 176–184 (2002).
8. Tadolini, B., Juliano, C., Piu, L., Franconi, F. & Cabrini, L. Resveratrol inhibition of lipid peroxidation. *Free Radic. Res.* **33,** 105 (2000).
9. Ana I. Romero-Pérez, Maite Ibern-Gómez, Rosa M. Lamuela-Raventós, * & and M. Carmen de la Torre-Boronat. Piceid, the Major Resveratrol Derivative in Grape Juices. *J. Agric. Food Chem.* **47,** 1533–1536 (1999).
10. Murias, M. *et al.* Antioxidant, prooxidant and cytotoxic activity of hydroxylated resveratrol analogues: structure–activity relationship. *Biochem. Pharmacol.* **69,** 903–912 (2005).
11. Leonard, S. S. *et al.* Resveratrol scavenges reactive oxygen species and effects radical-induced cellular responses. *Biochem. Biophys. Res. Commun.* **309,** 1017–1026 (2003).
12. Rice-Evans, C. a., Miller, N. J. & Paganga, G. Structure-antioxidant activity relationships of flavonoids and phenolic acids. *Free Radic. Biol. Med.* **20,** 933–956 (1996).
13. Cao, H. *et al.* Density functional theory calculations for resveratrol. *Bioorg. Med. Chem. Lett.* **13,** 1869–1871 (2003).

14. Neshchadin, D., Batchelor, S. N., Bilkis, I. & Gescheidt, G. Short-lived Phenoxyl Radicals Formed from Green-Tea Polyphenols and Highly Reactive Oxygen Species: An Investigation by Time-Resolved EPR Spectroscopy. *Angew. Chemie Int. Ed.* **53,** 13288–13292 (2014).

15. Neshchadin, D., Levinn, R., Gescheidt, G. & Batchelor, S. N. Probing the Antioxidant Activity of Polyphenols by CIDNP: From Model Compounds to Green Tea and Red Wine. *Chem. - A Eur. J.* **16,** 7008–7016 (2010).

16. Bolland, J. L. & Gee, G. Kinetic studies in the chemistry of rubber and related materials. III. Thermochemistry and mechanisms of olefin oxidation. *Trans. Faraday Soc.* **42,** 244–252 (1946).

17. Maillard, B., Ingold, K. U. & Scaiano, J. C. Rate constants for the reactions of free radicals with oxygen in solution. *J. Am. Chem. Soc.* **105,** 5095–5099 (1983).

18. Walling, C. & Gibian, M. J. Limiting Rates of Hydrocarbon Autoxidations. *J. Am. Soc.* **87,** 3361–3364 (1965).

19. Halliwell, B. How to Characterize a Biological Antioxidant. *Free Radic. Res. Commun.* **9,** 1–32 (1990).

20. Shadidi, F. & Wanasundara, P. K. J. Phenolic antioxidants. *Crit. Rev. Food Sci. Nutr.* **35,** 67–103 (1992).

21. Valgimigli, L. & Pratt, D. A. Antioxidants in chemistry and biology. *Encycl. Radicals Chem. Biol. Mater.* **3,** 1623–1677 (2003).

22. Ingold, K. U. Inhibition of the Autoxidation of Organic Substances in the Liquid Phase. *Chem. Rev.* **61,** 563–589 (1961).

23. Ingold, K. U. & Pratt, D. A. Advances in Radical-Trapping Antioxidant Chemistry in the 21st Century: A Kinetics and Mechanisms Perspective. *Chem. Rev.* **114,** 9022–9046 (2014).

24. Miller, N. J., Rice-Evans, C., Davies, M. J., Gopinathan, V. & Milner, A. A novel method for measuring antioxidant capacity and its application to monitoring the antioxidant status in premature neonates. *Clin. Sci. (Lond).* **84,** 407—412 (1993).

25. Whitehead, T. P., Thorpe, G. H. G. & Maxwell, S. R. J. Enhanced chemiluminescent assay for antioxidant capacity in biological fluids. *Anal. Chim. Acta* **266,** 265–277 (1992).

26. Wang, H., Cao, G. & Prior, R. L. Total antioxidant capacity of fruits. *J. Agric. Food Chem.* **44,** 701–705 (1996).

27. Whitehead, T. P., Robinson, D., Allaway, S., Syms, J. & Hale, A. Effect of red wine

ingestion on the antioxidant capacity of serum. *Clin. Chem.* **41,** 32–35 (1995).

28. Creasy, L. & Coffee, M. J. Phytoalexin production potential of grape berries. *J. Am. Soc. Hortic. Sci.* **113,** 230 (1988).

29. Chan, M. M. Antimicrobial effect of resveratrol on dermatophytes and bacterial pathogens of the skin $. **63,** 99–104 (2002).

30. Fabris, S., Momo, F., Ravagnan, G. & Stevanato, R. Antioxidant properties of resveratrol and piceid on lipid peroxidation in micelles and monolamellar liposomes. *Biophys. Chem.* **135,** 76–83 (2008).

31. Signorelli, P. & Ghidoni, R. Resveratrol as an anticancer nutrient: molecular basis, open questions and promises. *J. Nutr. Biochem.* **16,** 449–66 (2005).

32. FRANKEL, E. Inhibition of human LDL oxidation by resveratrol. *Lancet* **341,** 1103–1104 (1993).

33. Stojanovic, S., Sprinz, H. & Brede, O. Efficiency and Mechanism of the Antioxidant Action of trans -Resveratrol and Its Analogues in the Radical Liposome Oxidation. **391,** 79–89 (2001).

34. Li, D. *et al.* Hydroxyl Radical Reaction with trans -Resveratrol : Initial Carbon Radical Adduct Formation Followed by Rearrangement to Phenoxyl Radical. (2012).

35. Mahal, H. S. & Mukherjee, T. Scavenging of reactive oxygen radicals by resveratrol: antioxidant effect. *Res. Chem. Intermed.* **32,** 59–71 (2006).

36. Simon, H.-U., Haj-Yehia, A. & Levi-Schaffer, F. Role of reactive oxygen species (ROS) in apoptosis induction. *Apoptosis* **5,** 415–418

37. Das, P. K., Encinas, M. V & Scaiano, J. C. Laser flash photolysis study of the reactions of carbonyl triplets with phenols and photochemistry of p-hydroxypropiophenone. *J. Am. Chem. Soc.* **103,** 4154–4162 (1981).

38. Leigh, W. J., Lathioor, E. C. & St. Pierre, M. J. Photoinduced Hydrogen Abstraction from Phenols by Aromatic Ketones. A New Mechanism for Hydrogen Abstraction by Carbonyl n,π* and π,π* Triplets. *J. Am. Chem. Soc.* **118,** 12339–12348 (1996).

39. Evans, C., Scaiano, J. & Ingold, K. Absolute Kinetics of Hydrogen Abstraction from a-Tocopherol by Several Reactive Species Including an Alkyl Radical. *J. Am. …* **114,** 4589–4593 (1992).

40. Griller, D., Howard, J. a, Marriott, P. R. & Scaiano, J. C. Absolute rate constants for the reactions of tert-butoxyl, tert-butylperoxyl, and benzophenone triplet with

amines: the importance of a stereoelectronic effect. *J. Am. Chem. Soc.* **103,** 619–623 (1981).

41. Yoshihara, T. *et al.* Hydrogen atom transfer and electron transfer reactions in the triplet π π * state of 1{,}4-anthraquinone studied by CIDEP techniques and laser flash photolysis. *Phys. Chem. Chem. Phys.* **2,** 993–1000 (2000).

42. Scaiano, J. C. S. *Photochem.* **2,** 81–118 (1973).

43. Wagner, P. J. *Acc. Chem. Res.* **4,** 168–177 (1971).

44. Canonica, S., Hellrung, B. & Wirz, J. Oxidation of Phenols by Triplet Aromatic Ketones in Aqueous Solution. 1226–1232 (2000).

45. Rappoport, Z. *The Chemistry of Phenols: Part 1.* (Wiley, 2003).

46. Yoshihara, T. *et al.* Hydrogen atom transfer and electron transfer reactions in the triplet π,π* state of 1,4-anthraquinone studied by CIDEP techniques and laser flash photolysis. *Phys. Chem. Chem. Phys.* **2,** 993–1000 (2000).

47. Neyens, E. & Baeyens, J. A review of classic Fenton ' s peroxidation as an advanced oxidation technique. **98,** 33–50 (2003).

48. Fenton, H. J. H. LXXIII.-Oxidation of tartaric acid in presence of iron. *J. Chem. Soc.{,} Trans.* **65,** 899–910 (1894).

49. Zepp, R. G. Hydroxyl Radical Formation in Aqueous Reactions (pH 3-8) of Iron(I1) with Hydrogen Peroxide: The Photo-Fenton Reaction. 313–319 (1992).

50. Aveline, M., Kochevar, I. E. & Redmond, R. W. Photochemistry of the Nonspecific Hydroxyl Radical Generator , N -Hydroxypyridine-2 (1 H) -thione Be. **2,** 10113–10123 (1996).

51. Corvaja, C. in *Electron Paramagnetic Resonance: A Practitioner's Toolkit* (eds. Brustolon, M. & Giamello, E.) 3–36 (Wiley, 2009).

52. Gerson, F. & Huber, W. *Electron Spin Resonance Spectroscopy of Organic Radicals.* (Wiley-VCH, 2003).

53. Brustolon, M. & Giamello, E. *Electron Paramagnetic Spectroscopy.* (Wiley, 2009).

54. Yurkovskaya, A., Morozova, O. & Gescheidt, G. *Encyclopedia of Radicals in Chemistry, Biology and Materials.* (Wiley, 2012).

55. Gatlik, I., Rzadek, P. & Gescheidt, G. Structure-reactivity relationships in radical reactions: A novel method for the simultaneous determination of absolute rate constants and structural features. *J. …* 8332–8336 (1999). at

56. Goez, M. An Introduction to Chemically Induced Dynamic Nuclear Polarization.

Concepts Magn. Reson. **7,** 69–86 (1995).

57. Pine, S. H. Chemically induced dynamic nuclear polarization. *J. Chem. Educ.* **49,** 664 (1972).

58. Hayashi, H. *Introduction to Dynamic Spin Chemistry: Magnetic Field Effects on Chemical and Biochemical Reactions*. (World Scientific Publishing Co. Pte. Ltd., 2004).

59. Clancy, C. M. R., Tarasov, V. F. & Forbes, M. D. E. in *Electron Paramagnetic Resonance* (1998).

60. Slichter, C. P. *Principles of Magnetic Resonance. 2nd Edition*. (1978).

61. Kaptein, R. Simple rules for chemically induced dynamic nuclear polarization. *J. Chem. Soc. D* 732–733 (1971). doi:10.1039/C29710000732

62. Friebolin, H. *Basic One- and Two-Dimensional NMR Spectroscopy*. (Wiley-VCH, 2010).

63. Fiolhais, C., Nogueira, F. & Marques, M. *A Primer in Density Functional Theory*. (Springer, 2003).

64. Holthausen, M. & Koch, W. *A Chemist's Guide To Density Functional Theory*. (Wiley, 2001).

65. Duling, D. R. Simulation of Multiple Isotropic Spin-Trap {EPR} Spectra. *J. Magn. Reson. Ser. B* **104,** 105–110 (1994).

66. Becke, A. D. Density - functional thermochemistry . III . The role of exact exchange Density-functional thermochemistry . III . The role of exact exchange. **5648,** (2005).

67. Lee, C., Yang, W. & Parr, R. G. Development of the Colle-Salvetti correlation-energy formula into a functional of the electron density. *Phys. Rev. B* **37,** 785–789 (1988).

68. Weigend, F. & Ahlrichs, R. Balanced basis sets of split valence, triple zeta valence and quadruple zeta valence quality for H to Rn: Design and assessment of accuracy. *Phys. Chem. Chem. Phys.* **7,** 3297–305 (2005).

69. Kutzelnigg, W., Fleischer, U. & Schindler, M. in 165–262 (Springer Berlin Heidelberg, 1991).

70. Klamt, A. & Schuurmann, G. COSMO: a new approach to dielectric screening in solvents with explicit expressions for the screening energy and its gradient. *J. Chem. Soc.{,} Perkin Trans. 2* 799–805 (1993).

71. Neese, F. The ORCA program system. *Wiley Interdiscip. Rev. Comput. Mol. Sci.*

2, 73–78 (2012).

72. Figueiras, T. S., Neves-Petersen, M. T. & Petersen, S. B. Activation Energy of Light Induced Isomerization of Resveratrol. *J. Fluoresc.* **21,** 1897–1906 (2011).

73. Barone, V., Cimino, P. & Stendardo, E. Development and Validation of the B3LYP/N07D Computational Model for Structural Parameter and Magnetic Tensors of Large Free Radicals. *J. Chem. Theory Comput.* **4,** 751–764 (2008).

74. López-Nicolás, J. M. & García-Carmona, F. Aggregation State and pKa Values of (E)-Resveratrol As Determined by Fluorescence Spectroscopy and UV−Visible Absorption. *J. Agric. Food Chem.* **56,** 7600–7605 (2008).

75. Kaptein, R. Chemically induced dynamic nuclear polarization. VIII. Spin dynamics and diffusion of radical pairs. *J. Am. Chem. Soc.* **94,** 6251–6262 (1972).

76. Geimer, J. & Beckert, D. Study of radical pairs generated by photoreduction of anthraquinone-2 , 6-disulfonic acid with thymine by Fourier transform electron paramagnetic resonance. 24–26 (1998).

77. Pedersen, J. B. & Freed, J. H. Theory of chemically induced dynamic electron polarization. I. *J. Chem. Phys.* **58,** (1973).